SANDIA REPORT

SAND96-8516 • UC-404
Unlimited Release
Printed February 1996

Molecular Adhesion of a Polymer at a Metal Interface: Coupling of Quantum and Classical Forces

W. D. Wilson, C. L. Bisson, C. M. Schaldach

Prepared by
Sandia National Laboratories
Albuquerque, New Mexico 87185 and Livermore, California 94551
for the United States Department of Energy
under Contract DE-AC04-94AL85000

Approved for public release; distribution is unlimited.

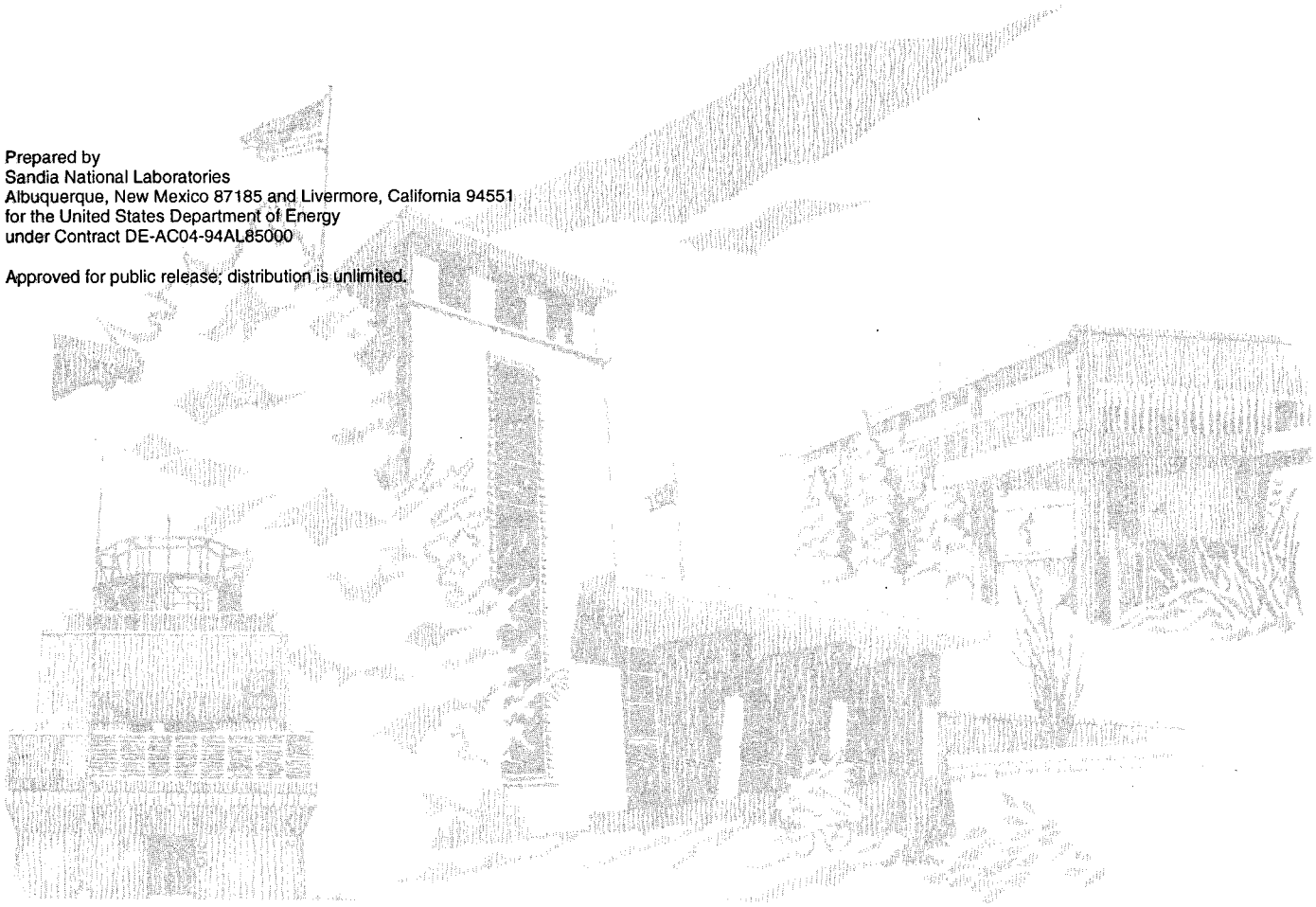

SF2900Q(8-81)

Issued by Sandia National Laboratories, operated for the United States Department of Energy by Sandia Corporation.
NOTICE: This report was prepared as an account of work sponsored by an agency of the United States Government. Neither the United States Government nor any agency thereof, nor any of their employees, nor any of the contractors, subcontractors, or their employees, makes any warranty, express or implied, or assumes any legal liability or responsibility for the accuracy, completeness, or usefulness of any information, apparatus, product, or process disclosed, or represents that its use would not infringe privately owned rights. Reference herein to any specific commercial product, process, or service by trade name, trademark, manufacturer, or otherwise, does not necessarily constitute or imply its endorsement, recommendation, or favoring by the United States Government, any agency thereof or any of their contractors or subconractors. The views and opinions expressed herein do not necessarily state or reflect those of the United States Government, any agency thereof or any of their contractors or subcontractors.

SAND96-8516
Unlimited Release
Printed February 1996

MOLECULAR ADHESION OF A POLYMER AT A METAL INTERFACE: COUPLING OF QUANTUM AND CLASSICAL FORCES

W. D. Wilson and C. L Bisson
Sandia National Laboratories
Livermore, California

and

C. M. Schaldach
University of California
Berkeley, California

ABSTRACT

The atomic reconfigurations of the simplest amino acid, glycine, at a realistic metal surface including a step and real surface charge are calculated. A boundary-element method for determining the polarization-induced binding enthalpy of molecules to metal surfaces in the presence of a dielectric is coupled to quantum chemical calculations of the gas-phase molecule. Enthalpies and potentially-derived fractional atomic charges are determined quantum mechanically using 6-31G** basis functions and MP2 level of theory for 216 different molecular configurations of glycine. A parameterized model is presented which captures the quantum results as a function of bond lengths, angles and dihedrals with an average deviation of <1 kcal/mole. The molecule and its substrate, an fcc metal slab, are discretized allowing heterogeneous dielectric interfaces which may change dynamically as the molecule approaches the surface. The slab is modeled as an explicit region of lattice atoms with corrections for its finite nature included using continuum theory. Real charge may be included on the surfaces, requiring the boundary conditions and hence the fundamental equations of Zauhar and Morgan to be modified. The results indicate that anionic glycine is bound to a Cu (100) surface with a binding enthalpy of ~1.7 eVand requiring the presence of a step of atomic dimensions, in a geometric configuration in agreement with experiments of Udval, et al. This binding is dramatically reduced in the presence of an intervening dielectric. At an atomically flat surface, neutral and zwitterionic glycine are found to be oriented with their N ends toward the neutral surface in agreement with experiment. These glycine molecules are furthermore found to undergo a critical phenomenon: Their molecular orientation "flips" by 180 degrees at a small, critical magnitude of real surface charge.

I. INTRODUCTION

A fundamental understanding of the biocompatibility of proteins with artificial implant materials has motivated experimental studies of amino acid adsorption on solid surfaces (1-5). Initial protein (perhaps blood fibrinogen) adsorption and subsequent surface-induced denaturization or change in conformation may activate clotting factors (factor XII) leading to rejection of the implant (6,7). Lundstrom and Salaneck (8) have concluded that an encouraging parallel exists between measurements of glycine in non-biological environments and the behavior of glycine in vivo. The reconfiguration of amino acid atoms at the surface provides an underlying key to our understanding of the initial events involved in the acceptance or rejection of the foreign material. Studies of the atomic reconfigurations of the simplest amino acid, glycine, at a well-characterized metal surface provide a first step.

Angle-dependent X-ray photoelectron spectroscopic measurements indicate that a glycine anion is adsorbed on a polycrystalline copper substrate (with a thermal desorption energy of ~1.5 eV) in a geometric configuration consistent with the two oxygen atoms and the nitrogen nearest the surface (2). This configuration involves a distortion from the ground state of the isolated molecule created by its interaction with the surface. This experimental conformation differs from that found for the zwitterionic form of glycine on hydrophilic gold, silicon and graphite where the nitrogen is found closest to the surface and the oxygens away from the interface (4,5). The zwitterionic (ZW) form of glycine does not exist in the gas phase (9,10) but can be stabilized by neighboring interactions. A neutral, nonionic (NE) form of glycine is stable, the two forms differing essentially by the motion of a proton from the NH3 group (ZW) to the nearby COO^- group (NE). The dipole moment of the ZW form is several times greater than that of the NE form which seriously affects its interaction with a polarizable interface.

Here we focus on the interaction of various forms of the glycine molecule with a polarizable interface discretized to allow for inclusion of realistic surface features such as steps and real (externally imposed) charge. The method also allows for a dielectric environment (second interface) between molecule and surface. The object is to develop techniques which can be bootstrapped to larger systems involving many amino acids; ab initio methods are limited to tens of atoms. We present coupled calculations of anionic glycine in which the electrostatic energy of the molecule in the presence of a polarizable surface is coupled to the intramolecular energy resulting from atomic distortions within the molecule. A commensurate model of the molecular intra-atomic potentials was obtained by fitting to the quantum-chemically (GAUSSIAN) -derived MP2-level energies of hundreds of geometrical configurations of anionic glycine as a function of bond lengths and angles, including dihedrals. A solvent-accessible surface and also a comparison atomically derived surface are constructed on a slab of the metal lattice to facilitate a boundary element solution to the Poisson equation. The electrostatic energy of each atom in the molecule resulting from its interaction with the metal surface is then found by integrating over the polarized interfaces between molecule, possible intervening dielectric, and metal surface. These surface-related intermolecular forces alter the configuration of the atoms within the molecule, the intramolecular energy associated with that alteration provided by the commensurate model.

The method of calculation and derivation of the linear equations involved in the boundary-element solution is described in Section II. In Section III, we describe the methods employed in the discretation of the surface and in Section IV we present the results of our calculations of the binding of anionic glycine in the presence of an atomic-scale step and also for neutral NE and ZW glycine in the presence of real surface charge. Section V contains a Summary and Discussion of the results.

II. METHOD OF CALCULATION

A molecule approaching a polarizable surface experiences electrostatic forces due to "real" surface charge and also the reaction field created by the polarization charge the molecule induces on the surface. ("Real" charge is to be distinguished from "bound" or "apparent" or "polarization" charges which are not able to be extracted from a dielectric; real or "true" surface charge is often a function of the pH of the medium because protons or hydroxyl ions from solution may be embedded in the surface.) Even a neutral molecule contains atoms which can be represented as having fractional charges (which sum to zero) each of which can give rise to induced polarization effects. The reaction electric field acts on the molecule to a) polarize its possible interface with the medium it may be embedded in and, b) to produce forces on the atoms which distort the molecule away from its equilibrium configuration. The relative movement of covalently bonded atoms in the molecule must be taken into account quantum mechanically making it necessary to couple the intramolecular to intermolecular force fields.

The total binding energy of the system, E_{tot}, relative to the molecule at infinity, is considered here to be comprised of E_{mol}, the energy of the molecule due to intramolecular forces relative to its equilbrium value; E_{es}, the electrostatic energy of interaction of each atom in the molecule with its surface boundary and any external interface; and E_{rep}, the repulsive interaction between atoms in the molecule and those in the surface region:

$$E_{tot} = E_{mol} + E_{es} + E_{rep} \qquad (1)$$

These energy terms are, of course, not independent: The atoms in the molecule relax due to electrostatic reaction forces and these ralaxations in turn effect the electrostatic forces, etc. The total energy must be minimized as a function of the relaxations through an iterative process.

The intramolecular energy, E_{mol} is obtained by calculating the MP2 energy of over 200 different geometric configurations of molecules in order to develop a parameterized model, reproducing the results of MP2 theory. The model is described in Section IIa. The electrostatic energy, E_{es}, is determined by a boundary-element solution to Poisson's equation, first involving the discretization of the surface. The method, described in Section IIb, enables inclusion of complex surface geometries and real charge. The repulsive energy of interaction between the atoms in the molecule and those in the surface, E_{rep}, is found by a rigid-atom local density technique described in Section IIc. We briefly describe the energy minimization technique in Section IId.

IIa. Intramolecular Interactions

We have optimimized the ground-state geometry of the neutral (NE), zwiterionic (ZW) and anionic (AN) forms of the glycine molecule at the Hartree-Fock level using 6-31-G** wavefunctions. Because the ZW form is found not to have a stable minimum in the gas phase, we employ the technique of Barone, et al. (9) of equalizing the N-H bond lengths in order to prevent reconfiguration into the NE form during the minimization process. We have furthermore optimized the wavefunctions at the Moller-Plosset -2 (MP2) level while fixing the nuclear coordinates. Results using GAUSSIAN (11), GAMMESS (12), and SPARTAN (13) were found to agree well with one another. Potentially-derived fractional charges for each ground state atom were obtained from these MP2 calculations; the results are given in Table I. The energies of the neutral nonionic (NE) and zwitterionic (ZW) forms of the glycine molecule are nearly identical; however, the dipole moment of the ZW form is nearly twice as large as for NE and will be shown to significantly effect its interaction with a surface. The three forms are plotted in Fig.1.

Motivated by the experiments of Udval, et al. (2), we calculated the enthalpy of formation of 216 different geometric configurations of the anionic glycine molecule, $CH_2NH_2COO^-$, forming a data set to be fitted by a parameterized model. Bond lengths, bond angles and dihedral angles were varied and the energy calculated at the MP2 level in each case. In general, bond lengths were varied by ±0.5 Å in steps of 0.01 Å and angles by ±70 degrees in steps of 10 degrees from equilibrium; for important dihedral angles, the variation was a full 360 degrees. Configurations resulting in energies greater than 0.2 Hartrees above the ground state were excluded, as were chemical reactions (changes in bonding).

A parameterized model was fitted to the ab initio results in order to speed the energy minimization calculations discussed later. Pairwise bond energies were fitted to a Morse potential,

$$E_m = b_3\{1+\exp(-2b_1(r-b_2))-2\exp(-b_1(r-b_2))\} \qquad (2)$$

Table II contains the Morse potential parameters determined by these fits to the ab initio data.

Atoms having N bonds to neighboring atoms, where N>=3, reside at the apex of the (N-1) triangles formed by the multiple bonds, the apex angles denoted θ_{123}, θ_{126} and θ_{127} on (carbon atom) 1 (see Fig.1a); by θ_{214} and θ_{215} on (carbon atom) 2; and by θ_{318} and θ_{319} on (nitrogen) atom 3. The subscripts denote the atoms forming the vertices of the triangles, the leading index being the apex angle. The energy relative to the ground state as a function of these apex angles (from the ab initio calculations), is then fitted to a polynomial,

$$\begin{aligned} E_\theta &= a_1(\theta-\theta_{eq})^2 + a_2(\theta-\theta_{eq})^4, \theta \le \theta_{eq} \\ E_\theta &= a_3(\theta-\theta_{eq})^2 + a_4(\theta-\theta_{eq})^4, \theta > \theta_{eq} \end{aligned} \qquad (3)$$

The angular coefficients, a_1- a_4, obtained are given in Table III.

By constructing normals to each of these triangles, the ab initio energy variation with dihedral angles, chosen to be the angles between these normals, can be captured. Rotational axes are along the bonds between the multiply-bonded (>3) atoms. Six dihedral angles so formed are defined in Table IV, the energy variation of the first five fitted to the functional form:

$$E(\Delta\varphi) = -\sum_{n=1}^{4} q_n(1-\cos^2 n\Delta\varphi) \qquad (4)$$

where $\Delta\varphi = \varphi - \varphi_{eq}$. The coefficients obtained, $q_1 - q_4$, are provided in Table IVa. The sixth dihedral angular variation was found to better fit the form:

$$E(\Delta\varphi) = \sum_{n=2}^{3} q_n(\cos n(\Delta\varphi - q_1) - \cos(q1)) \qquad (5)$$

The coefficients $q_1 - q_3$ are given in Table IVb.

In Fig.2 we have plotted the fitted energies versus the quantum-mechanically-derived energies relative to the equilibrium state (-283.0647785 a. u.) for all 216 molecules. The commensurate model fits the quantum (MP2) data set with an average deviation of <0.0017 a. u.

(~1 kcal/mole) and a maximum (in a C-O bond energy) deviation of ~0.01 a. u. (~6 kcal/mole). In Appendix B, we present plots of the MP2 energies and our model fits to these energies as a function of bond length, angles and dihedrals.

IIb. Electrostatic Interactions With the Surface

The electrostatic potential, $\phi(\mathbf{x})$, at a point, x, within a molecule whose surface separates the internal molecular region having a dielectric constant ε_1 from a region characterized by a different dielectric constant (e. g., a solvent) can be expressed as,

$$\phi(\mathbf{x}) = \frac{1}{\varepsilon_1}\int_V \frac{\rho(\mathbf{x}')}{|\mathbf{x}-\mathbf{x}'|}d^3x' + \sum_k \int_{S_k} \frac{\sigma^{tot}(\mathbf{x}')}{|\mathbf{x}-\mathbf{x}'|}d^2x' \tag{6}$$

where the first term represents the potential at **x** due to the charge distribution ρ(x) within the volume associated with the molecule and the second term the potential due to the real (σ^{real}) and polarization-induced (σ^{pol}) charge on each of the interface boundaries ($\sigma^{tot} = \sigma^{real} + \sigma^{pol}$). We have incorporated the first term above into the internal energy of the molecule, E_{mol}, and hence E_{es} is due only to charges on boundaries. Specifically,

$$E_{es} = \sum_1^N Q_i \phi_i(\mathbf{x}) \tag{7}$$

where terms involving σ^{pol} are multiplied by 1/2 to account for the energy required to induce the polarization charge.

We consider the case of multiple polarizable boundaries in a solvent dielectric medium. Each boundary encloses a molecule or solid; boundaries may intersect. In the derivation presented here, a boundary encloses a molecule impinging on a solid surface, the elements of the boundaries may intersect at small separations and hence form interfaces which change dynamically. Zauhar and Morgan (14) have derived the boundary element equations for treating interface polarization directly from boundary conditions on the electric displacement and electric field vectors mandated by Gauss's Law when no "real" charge exists on the interface. In the present work, Gaussian "pillboxes" are constructed at the interface in the usual manner and the discontinuity in the normal component of the displacement vector set equal to 4 π times the <u>real</u> charge density enclosed by the pillbox:

$$\mathbf{D}_{is}^p \bullet \mathbf{n}_i - \mathbf{D}_i^p \bullet \mathbf{n}_i = 4\pi\sigma_{is}^{real,p} \tag{8}$$

where $\mathbf{D}_{is}^p$ ($\mathbf{D}_i^p$) is the dispacement vector on the solvent side of (inside) the pth element of the ith interface and $\mathbf{n}_i^p$ is the outward (toward the solvent) normal to boundary i at p. Similarly, for the electric vector, this discontinuity is equal to 4 π times the <u>total</u> charge enclosed:

$$\mathbf{E}_{is}^p \bullet \mathbf{n}_i^p - \mathbf{E}_i^p \bullet \mathbf{n}_i^p = 4\pi(\sigma_{is}^{real,p} + \sigma_{is}^{pol,p}) \tag{9}$$

where $\mathbf{E}_{is}^{p}(\mathbf{E}_{i}^{p})$ is the electric vector on the solvent side of (inside) the pth element of the ith interface. In Eqs. (8) and (9), $\sigma_{is}^{real,p}$ and $\sigma_{is}^{pol,p}$ are the real and polarization (induced) surface charge densities. Assuming linear media,

$$\mathbf{D}_{is}^{p} = \varepsilon_{is}^{p}\mathbf{E}_{is}^{p} \tag{10a}$$

and,

$$\mathbf{D}_{i}^{p} = \varepsilon_{i}^{p}\mathbf{E}_{i}^{p} \tag{10b}$$

$\varepsilon_{is}^{p}(\varepsilon_{i}^{p})$ being the dielectric constant of the solvent region (region i interior) at its interface to boundary i at element p. Using Eqs. (1-3), we obtain,

$$\mathbf{E}_{i}^{p} \bullet \mathbf{n}_{i}^{p} = 4\pi\left(\frac{\varepsilon_{is}^{p}-1}{\varepsilon_{i}^{p}-\varepsilon_{is}^{p}}\right)\sigma_{is}^{real,p} + 4\pi\frac{\varepsilon_{is}^{p}}{\left(\varepsilon_{i}^{p}-\varepsilon_{is}^{p}\right)}\sigma_{is}^{pol,p} \tag{11}$$

which introduces the real surface charge (see Eq. (1) of ref.14).

The normal component of the electric field at element p within boundary i is given by,

$$\mathbf{E}_{i}^{p} \bullet \mathbf{n}_{i}^{p} = -2\pi\sigma_{is}^{tot,p} + \sum_{k=1}^{N_b}\sum_{j=1}^{N_k}\frac{1}{\varepsilon_k}\frac{Q_{jk}}{\left|\mathbf{r}_{ik}^{pj}\right|^3}\mathbf{r}_{ik}^{pj} \bullet \mathbf{n}_{i}^{p} + \sum_{k=1}^{N_b}\sum_{q\neq p}^{M_k} K_{ik}^{pq}\sigma_{ks}^{tot,q} \tag{12}$$

where $\sigma_{ks}^{tot,p} = \sigma_{ks}^{real,p} + \sigma_{ks}^{pol,p}$ is the total surface charge density at element p of boundary k. The first term on the right of Eq. (12) represents the self-field of element p; the second term is due to the N_k real point charges, Q_{jk}, within boundary k; N_b is the number of boundaries. This term need not be represented as a sum of atomic charges as Eq. (12) implies, but may be directly obtained as an integral over the actual charge distribution if it is known (e.g., from quantum calculations). M_k is the number of elements comprising boundary k. The last term in Eq. (12) represents the contribution to the normal component of the electric field at element p of boundary i from all other elements q on all boundaries k (including i). That is,

$$K_{ik}^{pq} = \int \frac{\mathbf{r}_{ik}^{p} \bullet \mathbf{n}_{i}^{p}}{\left|\mathbf{r}_{ik}^{p}\right|^3} dS_k^q \tag{13}$$

where dS_k^q is the differential associated with the area of element q of boundary k.

Solving Eqs. (11-12), we find,

$$\sigma_{is}^{pol,p} - f_i\sum_{k=1}^{N_b}\sum_{q=1}^{M_k} K_{ik}^{pq}\sigma_{ks}^{pol,q} = -\left(\frac{\varepsilon_{i}^{p}+\varepsilon_{is}^{p}-2}{\varepsilon_{i}^{p}+\varepsilon_{is}^{p}}\right)\sigma_{is}^{real,p} + f_i\sum_{k=1}^{N_b}\sum_{j=1}^{N_k}\frac{1}{\varepsilon_k}\frac{Q_{jk}}{\left|\mathbf{r}_{ik}^{pj}\right|^3}\mathbf{r}_{ik}^{pj} \bullet \mathbf{n}_{i}^{p} + f_i\sum_{k=1}^{N_b}\sum_{q\neq p}^{M_k} K_{ik}^{pq}\sigma_{ks}^{real,q} \tag{14}$$

which reduces to the Zauhar and Morgn (14) expression when the real surface charge is zero and when only one boundary is included. In Eq. (14),

$$f_i = \frac{\varepsilon_i - \varepsilon_{is}^{p}}{2\pi\left(\varepsilon_i + \varepsilon_{is}^{p}\right)} \tag{15}$$

For a single flat boundary in the absence of point charges it is easy to show that Eq. (14) gives the simple Gauss's Law result for a parallel plate capacitor. That is, in that case,

$$\sigma^{tot} = \frac{-2\sigma^{real}}{(\varepsilon_1 + \varepsilon_2)} \tag{16}$$

A point charge experiences an electric field of $2\pi\sigma^{tot}$ in the vicinity of a charged plane, the real charge being significantly reduced by the self polarization.

Similarly, Eq. (14) applied to the polarization charge density on a single flat surface having no real charge but reacting to a single point charge can be seen to agree with the solution using the method of images (15),

$$\sigma_{is}^{pol,p} = f_i \frac{1}{\varepsilon_i} \sum_j \frac{q_j}{\left|\mathbf{r}_{ik}^{pj}\right|^3} \mathbf{r}_{ik}^{pj} \bullet \mathbf{n}_i^p \tag{17}$$

Eqs. (14) may be recognized as a set of linear equations,

$$\{[\mathbf{I}] - f[\mathbf{K}]\}[\sigma] = \left[\mathbf{T}^{real}\right] \tag{18}$$

which may be solved by the usual methods of linear algebra.

IIc. Repulsive Interatomic Interactions

The interatomic interaction between the atoms of the glycine molecule and the Cu atoms of the surface were calculated using a rigid-atom local density technique (16). The electron distributions are calculated quantum mechanically (in the Hartree-Fock-Slater approximation (17)) and the classical electrostatic energy of interaction between these overlapping distributions obtained. Corrections for the increase in kinetic $\rho^{\frac{5}{3}}$ and exchange $\rho^{\frac{4}{3}}$ energy in the overlap region are included. Such potentials provide a good approximation to the interactions between molecules when chemical binding is not significant.

In Fig 3 we have plotted the energy of interaction of a neutral Cu atom with the C, N, O, and H atomic constituents of glycine. We fitted the results to a useful functional form (to within $\sim 10^{-4}$ eV) and present the parameters in Table V. The functional form is not meant to convey physical meaning but only a numerical convenience.

IId. Coupling: Energy Minimization

If the molecular bond lengths and angles are held fixed, the intramolecular potential can be neglected and an approximate minimum energy configuration determined. When atomic relaxations are to be included, an iterative procedure is employed: the gradient of the total energy with respect to the cartesian coordinates of the center of mass and three Euler angles defining rotation about that center is determined (stepsize of ~0.002 a. u. and ~0.5 deg, respectively), and the molecule then repositioned along that gradient. Successive gradients are then determined which ultimately vanish as the energy approaches a minimum.

III. DISCRETATION OF THE SOLID SURFACE

The discretation of the surfaces can be performed in a number of ways (18). We have employed two methods for discretizing surface lattice atoms to form a subset or "slab". In the first method, the slab is viewed as a macromolecule in much the same way as our "solvent-accessible surface" technique described in Appendix A. Briefly, an N x N plane of lattice atoms (spheres) is sliced into (imaginary) planes along one axis. A "solvent" ball is then rolled over; i.e., completely around, each plane forming surface "dots." Triangles are then formed from the dots and areas and normals are then associated with the dots. The dots having negative normals are then eliminated from the list, finally leaving a set of coordinates, normals and areas for dots on the "top" surface of the slab of lattice atoms. We refer to this model of the dot structure as the molecular surface model (MSM). The number of planes, the solvent ball radius, and the number of pieces the ball is divided into may then be varied to obtain more or less dots. Fig. 4a shows the dot structure for an fcc (100) plane of 17 x 17 atoms sliced by 65 planes producing 1900 dots.

An alternative scheme begins by placing one dot at the top pole of each lattice atom. N dots are thus formed which may be accurate enough for some purposes. By rotation of $\pm\phi$ about, say, the x axis (z pointing up from the slab), each of these N dots (one per atom) can be split into three or more dots per atom; further rotations about the y axis could further split these dots. The surface details are captured in the dot structure as more dots are included on each atom. The angles can be varied and the number of dots in each direction also varied using this technique. This method does not include a solvent ball and hence does not have dots on "bridging" sites. We refer to this model of the dot structure as the atomic surface model (ASM). Fig. 4b shows the dot structure for an fcc (100) plane of 17 x 17 atoms with three dots per atom, producing 432 (upward) dots.

Model calculations of the electrostatic energy of a single positive point charge as a function of distance above the surface (dielectric constant $\varepsilon 2=100$ (19, 20)) are presented for three MSM and two ASM dot structures in Fig. 5. Comparison with the continuum analytical (image method) solution indicates the expected convergence for large separations. The continuum result is obtained by integrating the induced charge density divided by the distance to the charge over an area of the infinite plane equal to that of the slab; it represents a direct comparison of the potentials for similar footprints. In the near surface region (~3-10 Bohrs), the discretized surfaces agree well with one another and lie consistently above the continuum result. At extremely close separations (<~2 Bohrs), the single dot per atom approximation (ASM:S5) exhibits a turning up, indicating its inappropriateness for very-near-surface calculations. For distances greater than ~ 5 Bohrs, however, this same surface provides potentials most closely resembling the continuum result. Because of its reasonable size and behavior, we chose the MSM method for a 17 x 17 slab for the glycine calculations presented below.

The continuum model was also used to provide an estimate of the errors involved in choosing the atomistic slab sizes. The potential energy due to a system of point charges q_i at

x_i, y_i, z_i (z_i normal to the slab; origin at the center of the slab), due to the polarization charge they induce on those regions of the "infinite" lattice which lie outside the slab, can be calculated from,

$$W_{out} = \frac{f_i}{2\varepsilon_i} \sum_{i,j} q_i q_j \left\{ \frac{\pi}{\left[(x_j - x_i)^2 + (y_j - y_i)^2 + (z_j + z_i)^2\right]^{\frac{1}{2}}} - \int_{-b}^{b}\int_{-b}^{b} \frac{z_j dxdy}{\left[(x_j - x_i)^2 + (y_j - y_i)^2 + z_j^2\right]^{\frac{3}{2}} \left[(x_j - x_i)^2 + (y_j - y_i)^2 + z_i^2\right]^{\frac{1}{2}}} \right\} \quad (19)$$

where -b and b are the slab boundaries. This correction potential increases with distance from the lattice and for large x and y. The finite-slab correction is < 0.002 a. u. for our 17 x 17 atom slab for charges within z ~20 Bohrs no more than ~10 Bohrs from the origin in the xy plane. Within this zone corrections are small; outside the zone corrections are not difficult to include. For a small slab, such as employed in quantum cluster calculations, these polarization corrections may be important.

In the intersection model considered here, the molecular boundary intersects the slab boundary when there is insufficient space for water (or other dielectric) molecules between them. Elements comprising the slab boundary within the footprint of the molecule then change their dielectric interface from that of the solvent to that of the molecule. Dots on the molecular boundary lying closer than a characteristic distance (~1 Bohr) are eliminated. The heterogeneous molecular boundary then appropriately interfaces partially to the solvent and partially to the solid.

The position of the molecular surface of dots which, for a completely flat surface, can be compared to the position of the classical image plane. Finnis (19) has performed density functional theory calculations on aluminum and compared them with a discrete classical model. He concluded that the effect of atomic structure is to pull the image plane inwards with respect to its jellium value, specifically to ~0.875 of the atomic radius, r_0. Duffy, et al (20) then used this value in their metal-to metal-oxide interface calculations. Based upon this work, we placed our molecular surface at 0.875 of the copper atomic radius (r_0=4.307 Bohrs).

IV. RESULTS: A. ANIONIC GLYCINE AT A STEP

We find the minimum energy configuration of anionic (AN) glycine on an atomically flat (100) copper surface to have its nitrogen atom up, away from the surface and its oxygen atoms nearest to the interface. Induced polarization effects create a binding enthalpy to the surface of ~0.053 a. u. (~1.4 eV) within the range of experimental thermal desorption measurements. Atomic reconfigurations within the molecule produced by interface forces do not significantly alter the basic AN configuration. As noted in the introduction, this N-up geometry disagrees with experiment (2).

The situation is strikingly altered, however, in the presence of a surface step of one atomic spacing. This geometrical defect introduces additional polarizable interfacial area which stabilizes the nitrogen atom as well as one of the oxygen atoms in the glycine at the step interface as shown in Fig. 6. (A second interface is shown in Fig. 6 surrounding the molecule for reasons

to be discussed below.) We denote this molecular configuration of anionic glycine at a step as ANS. The hydrogens in the amine rotate away from the step, exposing the nitrogen's large negative charge. This configuration has the O, O and N of glycine essentially down on the surface in agreement with the X-ray photoemission spectroscopic (XPS) experiments. The interface component of the binding enthalpy becomes ~-0.087 a. u., sufficient to overcome the ~0.025 a. u. intramolecular energy required to distort the molecule. The total binding enthalpy becomes ~-0.062 a. u. (~1.7 eV), lower than that for a flat surface and consistent with thermal desorption and XPS measurements. This configuration is a direct result of atomic relaxations near the surface step.

In Fig. 7, we have plotted the energy of this ANS molecule, frozen in its minimum energy (near step) configuration, as a function of distance from the surface. Note the energy in the single boundary case approaches zero at large separations.

If the glycine were surrounded by a dielectric medium, such as a protein, however, a second polarizable interface would exist which could influence the binding. Also in Fig 7, therefore, we have plotted the energy of the ANS configuration in the presence of a dielectric rather than vacuum, that is, when a second polarizable interface surrounding the molecule is introduced. As nodes (dots) on the molecular boundary approach nearer than some critical limit, r_1, of the <100> surface, those dots are removed from the molecular surface. The slab surface is then exposed to the charges within the molecule albeit there remains an "umbrella" interface comprised of the remaining dots (see Fig.6). It can be seen that the dielectric ($\varepsilon 2=2$) provides nearly complete screening of the anion and a significant lowering of the magnitude of the interaction with the surface; the binding enthalpy is reduced to ~0.4 eV (see Fig.7). The measured binding energy (~1.5 eV) is therefore consistent with a high vacuum although some screening cannot be ruled out.

Note that the energy ($\varepsilon 2=2$) in Fig.7 at large separations asymptotically approaches the electrostatic solvation (Born) energy of the ANS molecule (-0.0449 a. u.), rather than zero. This value was separately determined for the molecule in its ANS configuration in a dielectric medium having $\varepsilon 2=2$. (Note in Table I this Born energy is given for the AN configuration in water, ε~81.)

B. Nonionic and Zwitterionic Glycine

The model predicts a critical phenomenon to occur as a function of real surface charge which can be understood from basic electrostatics. We find the minimum energy configurations of the neutral NE and ZW forms of glycine are weakly bound to a <u>neutral</u> metal surface with the nitrogen (N) down and the COO group up, away from the surface, in agreement with experiment (4,5). Atomic relaxations within the molecules are not included for these weakly bound species. The dipole moments, ground-state MP2 energies and Born energies are given in Table I. The introduction of a small positive surface charge has little effect until, at a critical magnitude, σ_{cr}^{real}, it causes these molecules to "flip" 180 degrees so that N is up and the COO group down, nearest to the surface (Fig. 8). Resultantly, the minimum distance of the nearest atom to the surface, z_{min}, is also abruptly changed at this critical real charge density. The energy and minimum distance to the surface versus real surface charge is presented in Fig. 9 for the NE form where the critical phenomenon is apparent. Results for the ZW form exhibit the same basic characteristics; σ_{cr}^{real} for this form is less (~0.7 μCoul/cm^2), consistent with its larger dipole moment.

The results can be understood by considering the neutral (NE) and zwitterion (ZW) forms as approximate dipoles and the surface as an infinite flat sheet of charge (in, say, the xy plane).

Such a surface gives rise to a constant electric field ($2\pi\sigma^{tot}$) independent of distance from the plane (i. e., independent of z). A perfect dipole directed along the normal to the surface in the field of a positively charged surface is in a state of unstable equilibrium when its positive charge is nearest the surface; small motions result in a reorientation due to the torque.

The NE form of glycine acts roughly like an imperfect dipole with positive charge (~+0.064) above a plane bisecting the carbon atoms (i. e., near N) and equal negative charge below this plane. A small positive surface charge therefore flips the molecule from its neutral-surface-N-down position into a lower energy configuration having N up. Its actual minimum energy configuration is determined by the balance of electrostatic and repulsive (atom-atom) forces. From another point of view, in its neutral-surface-N-down position, NE induces a negative polarization charge on the surface which binds the molecule. The introduction of real positive surface charge adds to this surface charge serving to reduce this binding. The ZW form acts essentially the same but has a larger dipole moment (see Table I) and hence requires correspondingly less surface charge to reorient it.

Although the details of the ZW form chosen here will effect the value of σ_{cr}^{real}, the basic dipolar behavior will remain. It is interesting to ascertain, however, whether the effect of a surrounding medium might stabilize the ZW form. The Born energy of the neutral NE and ZW forms of glycine in water are given in Table I (obtained using a molecular surface of comprised of 17 planes with a solvent ball (see Appendix A) of radius 2.27 Bohrs and 23 pieces generating 687 dots on the ZW surface). The calculation uses the fixed, potential-derived charges in Table I. We find that the Born energy of the ZW form, although greater in magnitude than that for NE, is insufficient to account for the ZW being preferred over the NE in water. It is to be recognized, however, that here we do not iterate the electronic structure calculation with the Poisson solution in the presence of the solvating surface, a method employed by Melius and Colvin (21).)

V. SUMMARY AND DISCUSSION

We have calculated the reconfigurations of various forms of glycine molecule in the presence of a realistic surface and predict the presence of a polarizable step to account for the experimental anionic configuration. It has been experimentally known for some time that surface defects such as steps can increase surface binding. Christmann and Ertl found that hydrogen adsorption at sites associated with steps on a a Pt (111) surface takes place with a higher binding energy (22). They postulated that relatively high electric fields exist near the steps which polarize the incoming molecules thereby introducing a torque which influences their orientation. In the case of glycine treated here, polarization-induced atomic relaxations are responsible for the reconfiguration (and may indicate their contribution to adsorbed protein denaturing and biological response). The calculated binding energy is consistent with thermal desorption measurements on adsorbed glycine in an ultra-high vacuum. Calculations aimed at estimating the possible role of an intervening dielectric indicate a very significant screening would take place.

The nonionic (NE) and zwitterionic (ZW) forms of glycine are found to undergo a critical phenomenon: the molecules "flip" their orientation 180 deg from N down (O up) to N up (O down) at a small critical magnitude of real surface, ~ 2 μ Coul/cm^2 for NE and ~0.7 μ Coul/cm^2 for ZW, behavior which may influence chemical interactions on surfaces.

The results have more general implications in that similar forces to those created by a polarizable step could be formed from other surface features (neutral impurities, grain boundaries, etc.). Furthermore, real surface charge can exist in very different geometries and forms other than uniform "smearing" of the charge as modeled here (e.g., point charges, oxides).

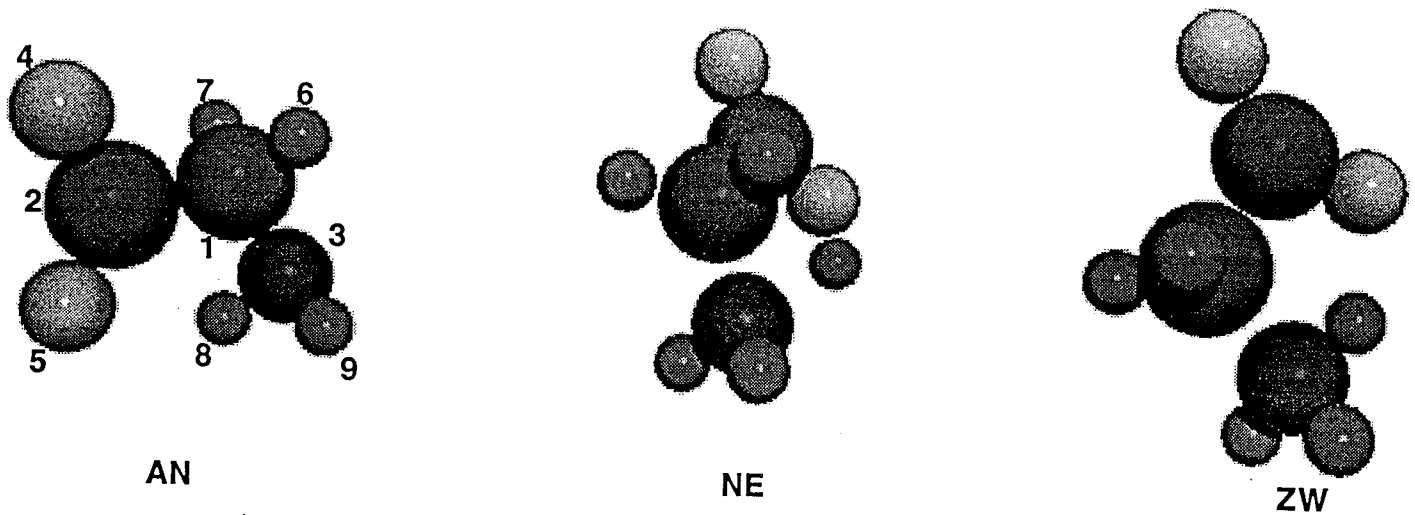

Figure 1. Ground state configurations of anionic (AN), neutral nonionic (NE) and zwitterionic (ZW) glycine molecules determined at the Hartree-Fock level. Note the motion of the H atom from O (in NE) to N (in ZW), there forming a symmetrical NH3 fragment (8). Energies and fractional charges calculated at the MP2 level are given in Table I.

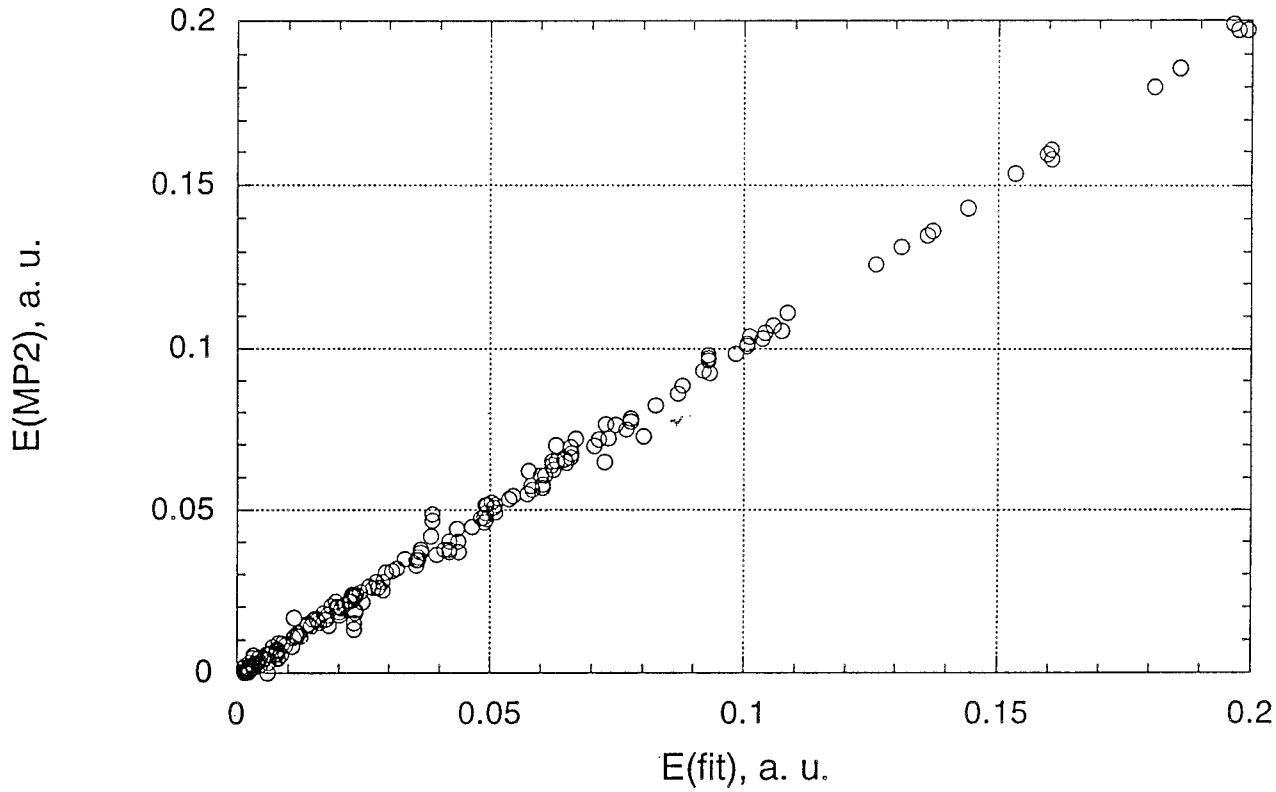

Figure 2. Comparison of the calculated and fitted energies of 216 different geometric configurations of the anionic (AN) glycine molecule relative to the equilibrium state. The ordinate represents the MP2/631G** quantum (GAUSSIAN) result; the abscissa the commensurate model fits to these energies. The average error in the fitted energies is <~1 kcal/mole.

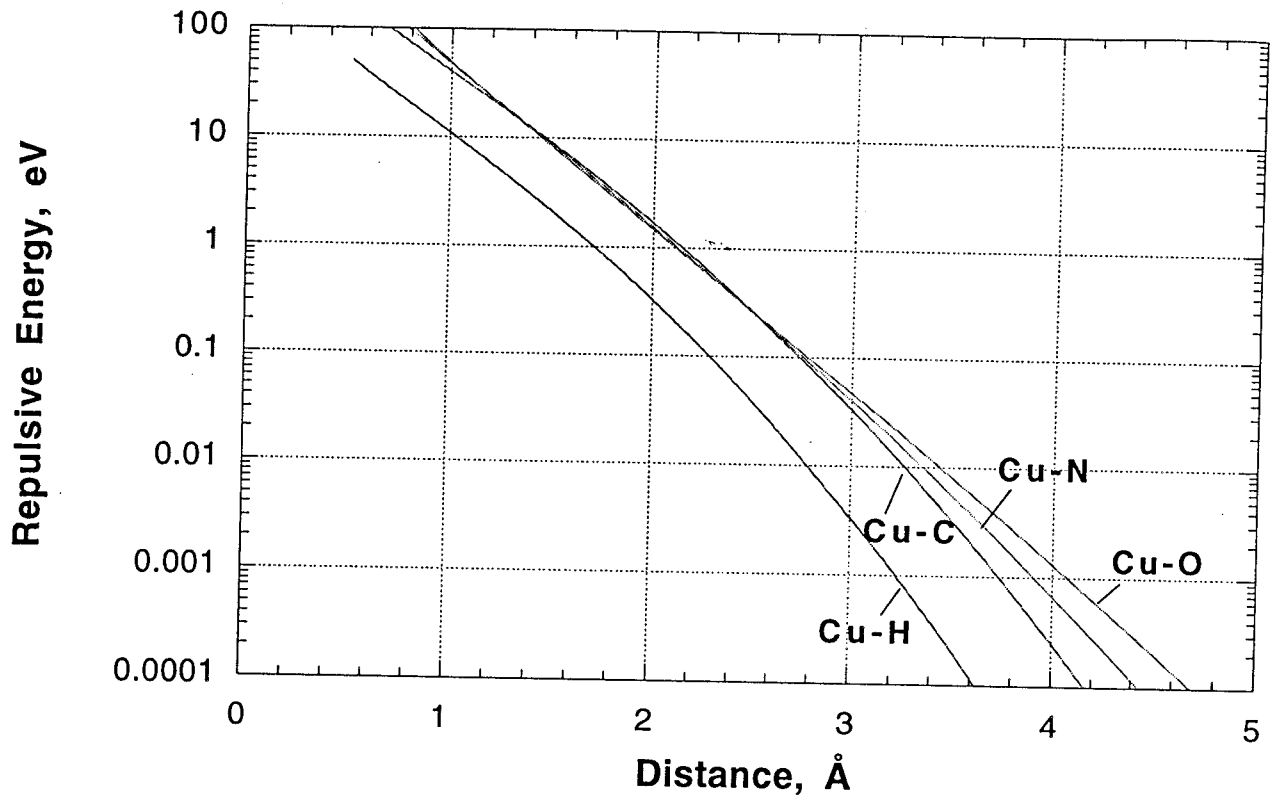

Figure 3. Repulsive interaction between neutral surface Cu atoms and atoms in the glycine molecule determined by local density calculations (16). Fits to these potentials are given in Table V.

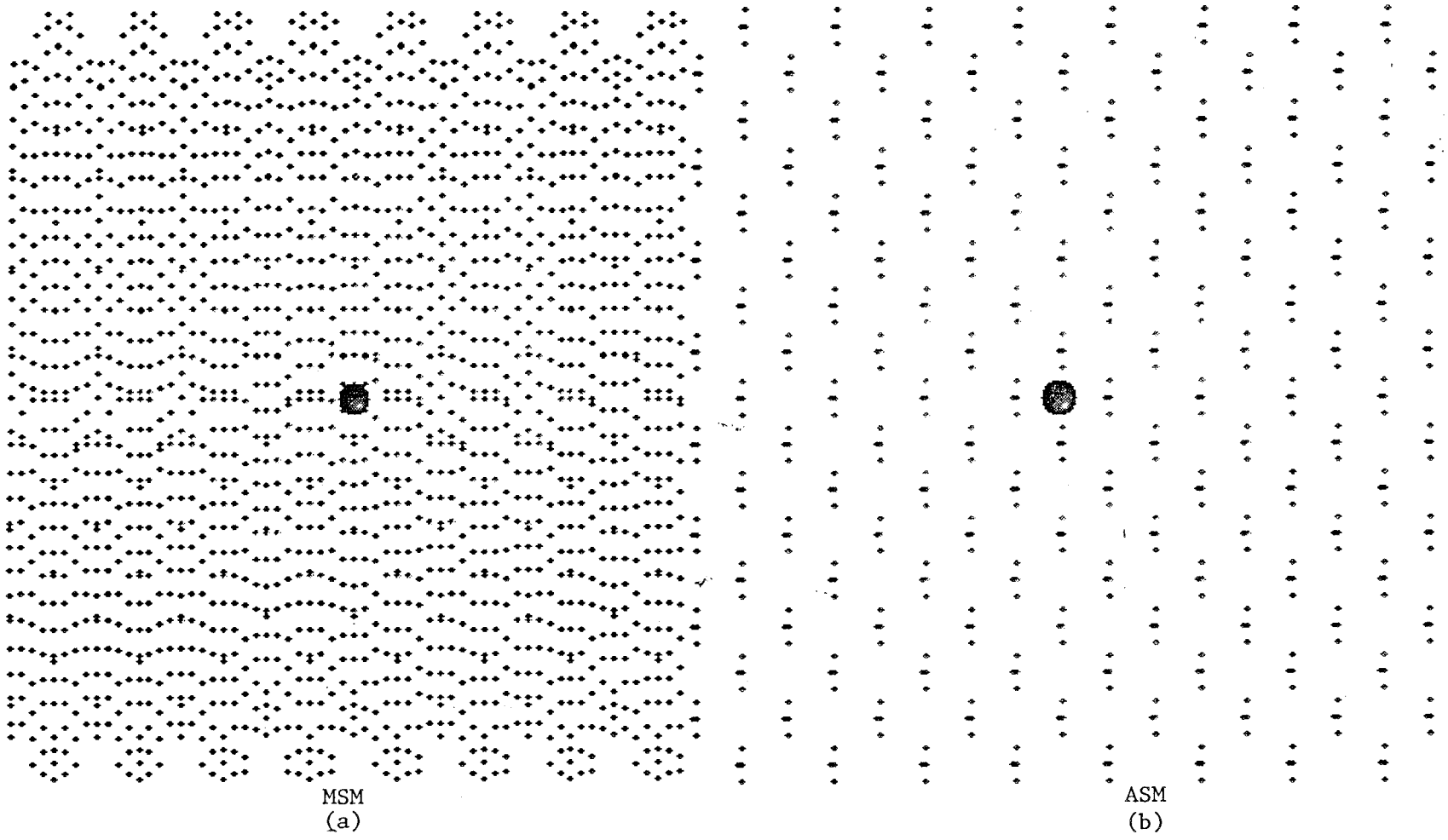

Figure 4. Comparison of slab discretation models. The molecular surface model (MSM) of discretation for 1900 dots on the left and the atomic surface model (ASM) for three dots per atom is shown on the right. A point charge in shown at the origin in this top view (see Fig. 5).

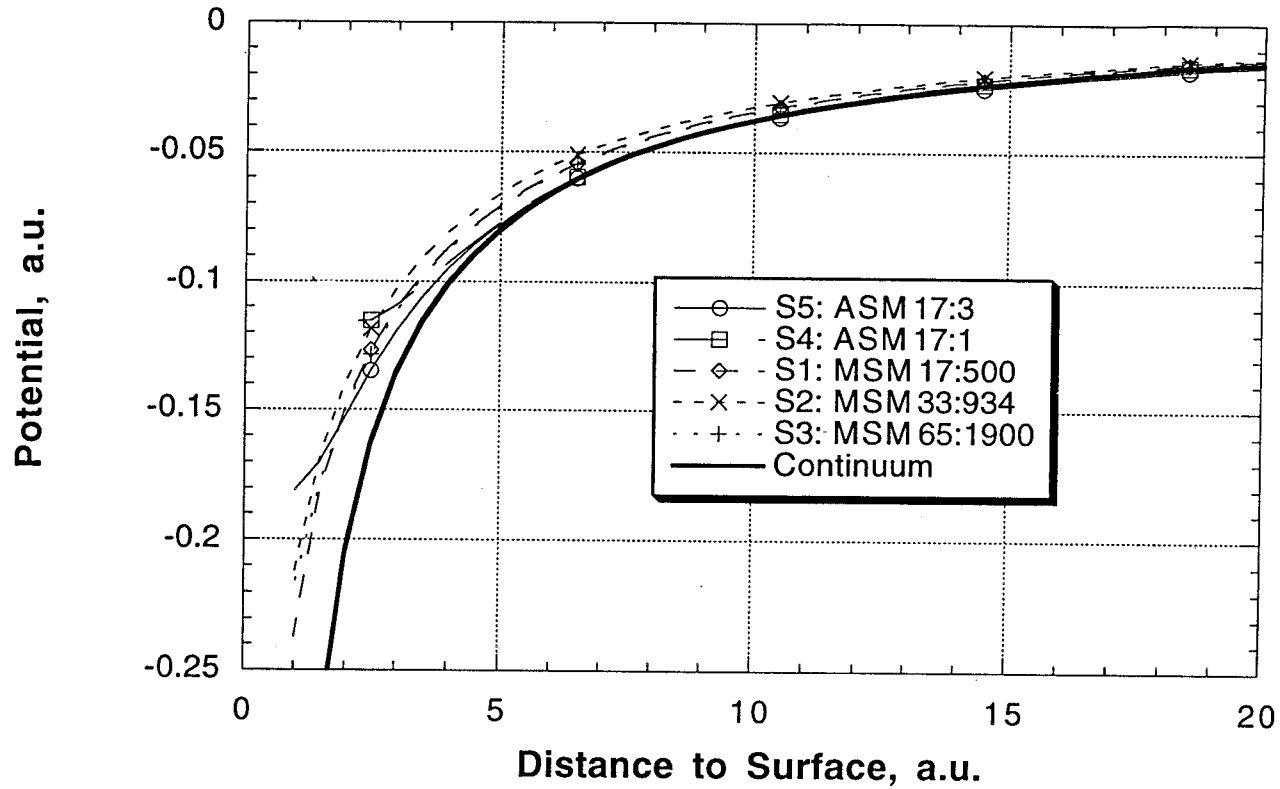

Figure 5. Electrostatic potential due to (and at) a point charge as a function of distance to the surface. The surface is discretized using an atomic surface method (ASM) on a slab of 17 x 17 lattice atoms each of which has three dots (S5) or one dot (S4) and also a molecular surface method (MSM) for 17, 33, or 65 planes of atoms giving rise to 500 (S1), 934 (S2) or 1900 (S3) dots. The atomistic curves all lie above the continuum (image) result and diverge at very short separations while converging at distances >~10 a. u.

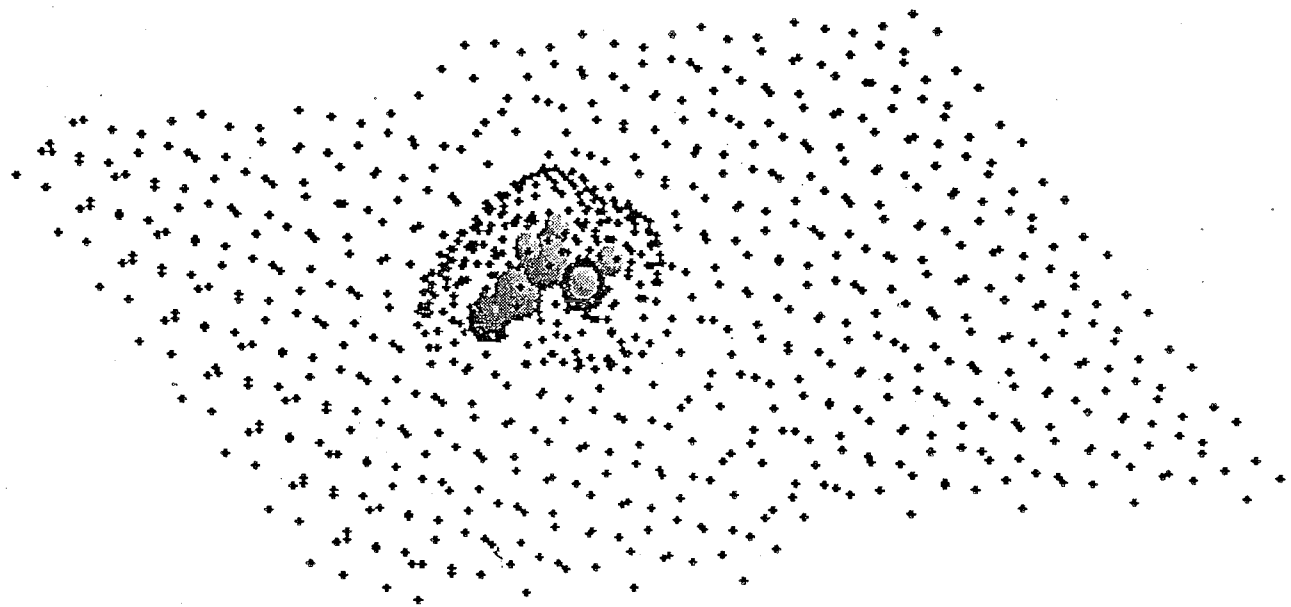

Figure 6. Minimum energy configuration of anionic glycine (ANS) at a step on a <100> Cu surface. The configuration results from atomic relaxations brought about by the additional induced polarization (reaction electric field) of the step. Note the "down" orientation of the O atoms and the N atom, in agreement with XPS measurements (2). The molecule is shown encapsulated in an additional molecular surface which provides an interface to a possible intervening dielectric.

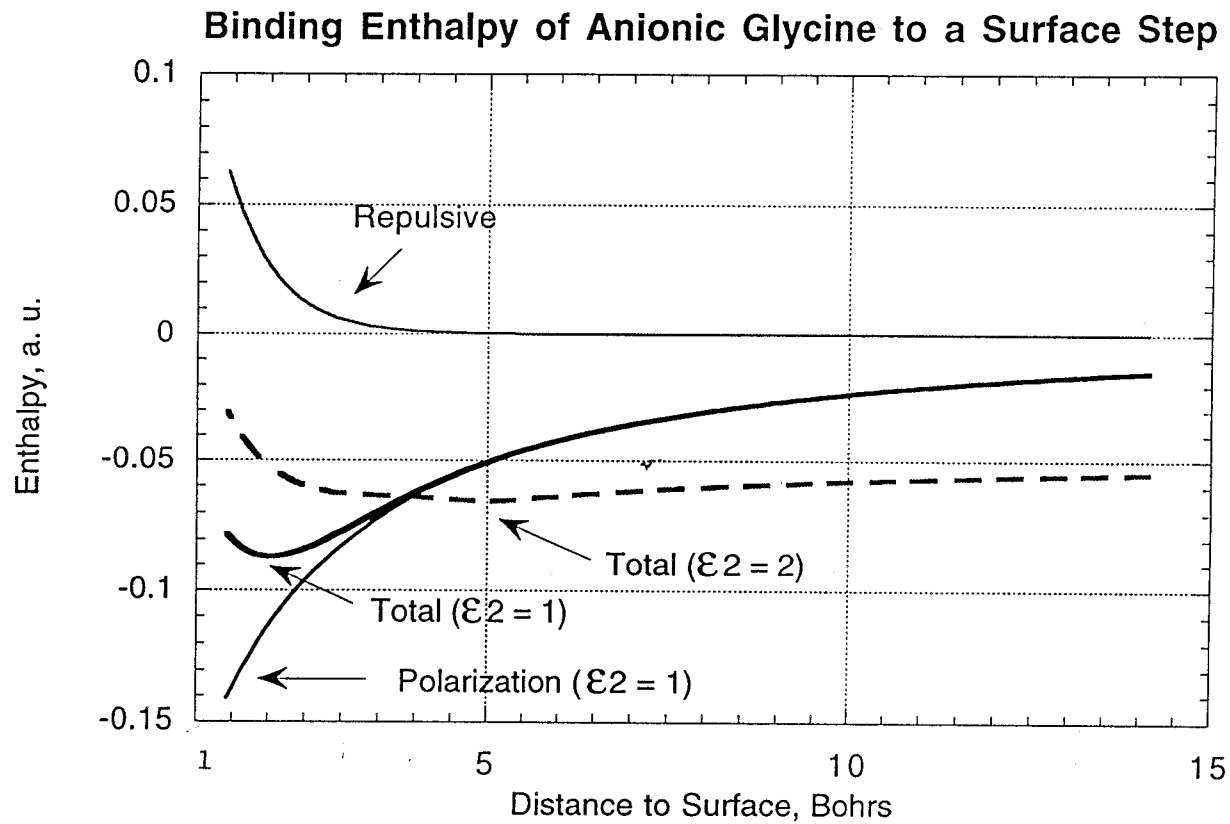

Figure 7. Binding enthalpy of anionic glycine (ANS) as a function of distance to a step on a <100> Cu surface. ε_2 (=2) is the dielectric constant of the surrounding dielectric medium; the molecule approaches its Born Energy (-0.0449 a. u.; ANS state) at large separations. Note that the binding enthalpy of the screened molecule is reduced to ~0.016 a. u. (~0.4 eV) by the dielectric.

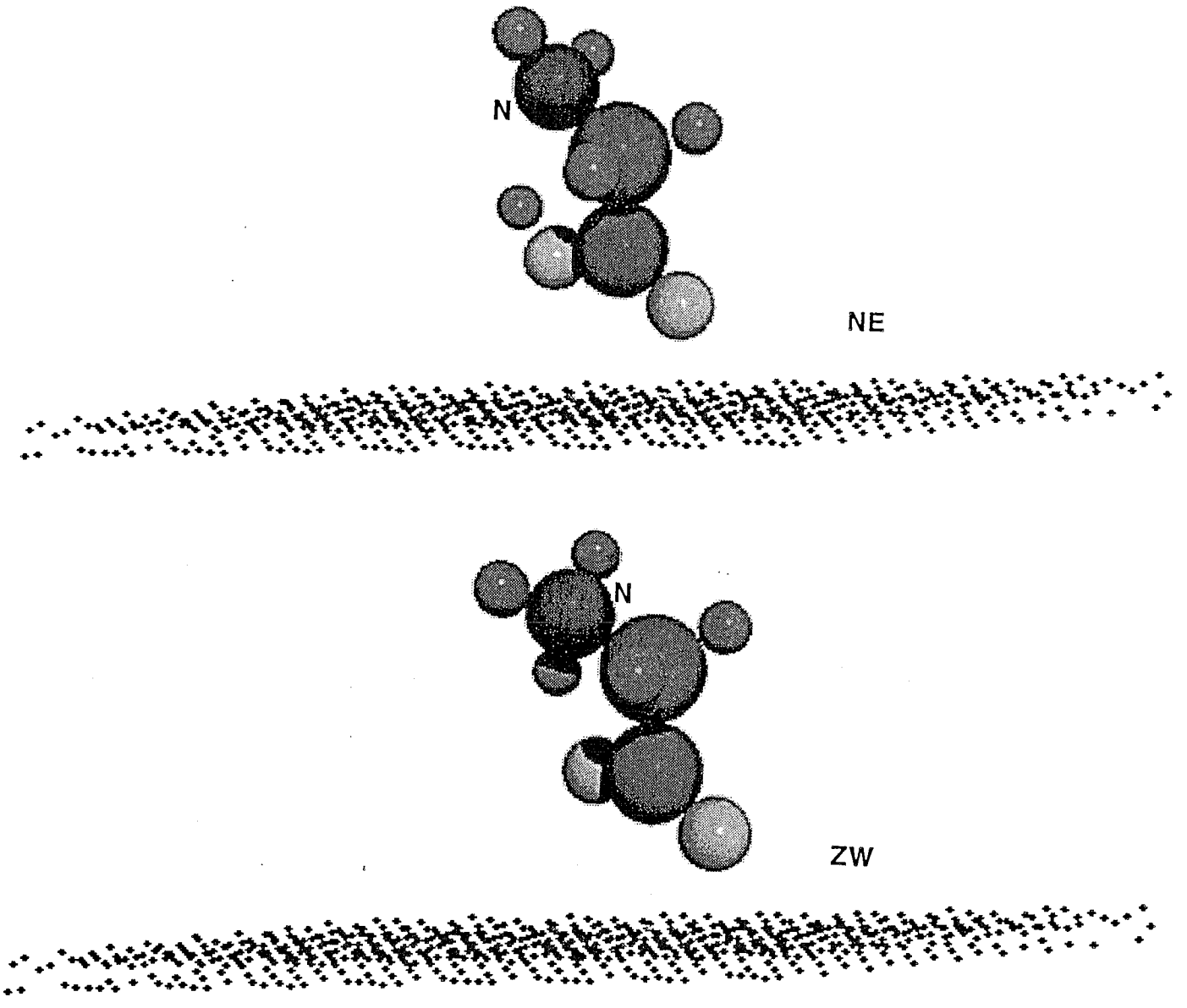

Figure 8. Minimum energy configurations of neutral (NE) and zwitterionic (ZW) forms of glycine on a positively charged surface, with $\sigma^{real} > \sigma_{cr}^{real}$ in each case. Note the N-up configuration is obtained, resulting from the 180 deg surface-charge-induced reorientation.

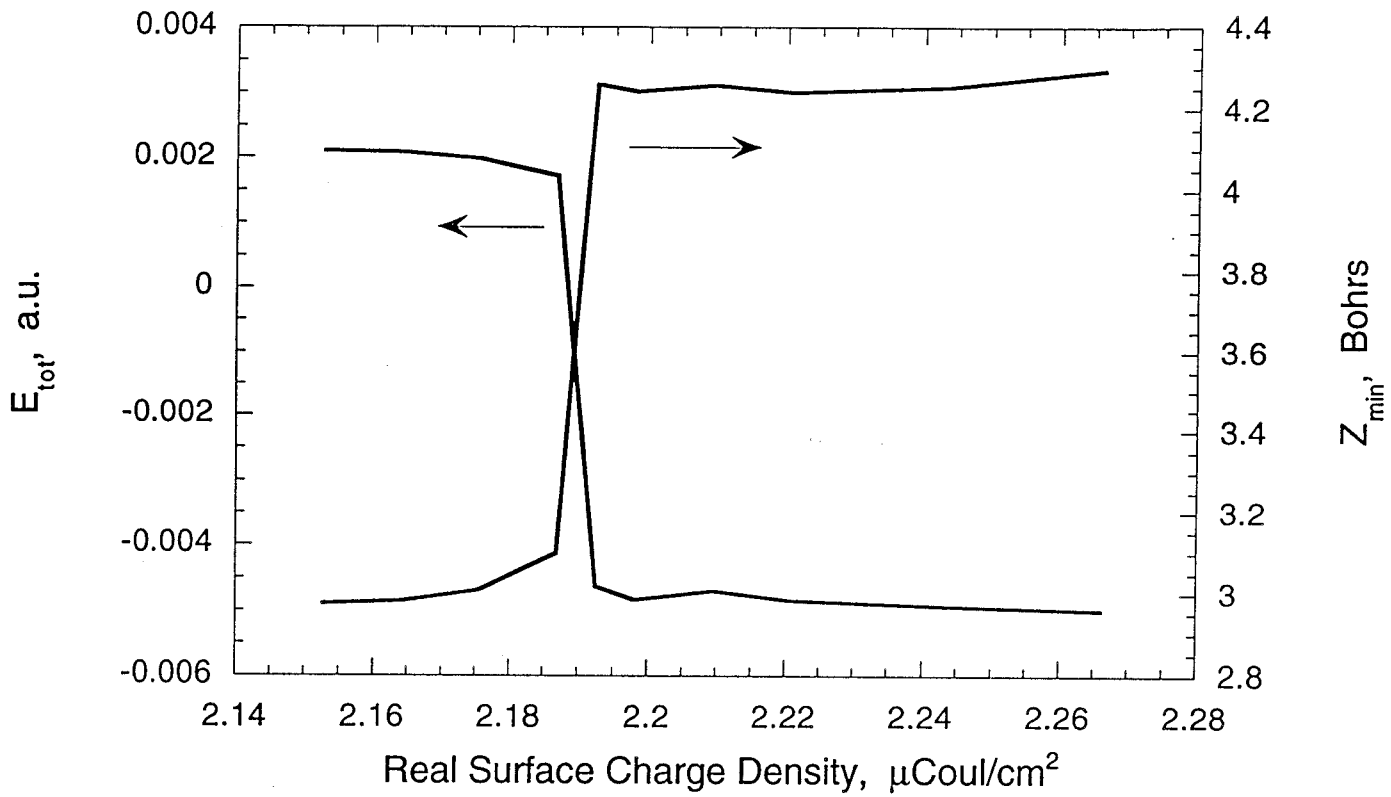

Figure 9. Energy versus σ^{real} for the NE form of glycine on a <100> Cu surface. Note that at σ_{cr}^{real}, the energy is dramatically lowered due to a sudden180 deg reorientation ("flipping") of the molecule. The minimum distance to the nearest atom to the surface, σ_{cr}^{real}, also makes a jump at σ_{cr}^{real}.

Table I. Atomic Charges, Molecular Configurational Energies, and Dipole Moments for equilibrium configurations of Glycine. Subscripts on atoms in column 1 correspond to atom numbers for the anionic form given in Fig. 1a.

Atom	Neutral(NE)	Anion	Zwitterion(ZW)
N3	-0.948482	-1.016859	-0.542970
C_1	0.300566	0.388044	-0.045894
C_2	0.756121	0.795172	0.750683
O_5	-0.614396	-0.821306	-0.678238
H_9	0.365879	0.337859	0.326361
O_4	-0.567910	-0.858241	-0.635245
H_8	0.367669	0.321722	0.343183
H_7	-0.031682	-0.081183	0.069486
H_6	0.007514	-0.065208	0.069445
H_{10}	0.364721		0.343188
Energy (RHF), a.u.	-282.8435	-282.2644	
Energy (MP2), a.u.	-283.6405	-283.0648	-283.6083
Dipole Moment, Debye	5.70	3.95	9.43
Born Energy, a. u. (water)	-0.0091	-0.0852	-0.0224

Table II. Morse Potentials for Bonds in Glycine

Parameter	C_1-H	C_1-N	C_1-C_2	N-H	C_2-O
b_1 (Bohrs^{-1})	1.07203	1.00570	1.07992	1.23844	1.70289
b_2 (Bohrs)	2.07087	2.78758	2.97635	1.93094	2.39614
b_3 (a.u.)	0.07768	0.08756	0.05271	0.08082	0.06166

Table III. Angles Fitted with Polynomials

Parameter	θ_{123} C_1-C_2-N3	θ_{126} C_1-C_2-H_6	θ_{127} C_1-C_2-H_7	θ_{214} C_2-C_1-H_4
a_1 (a.u. /rad^2)	0.183211	0.095134	0.104050	0.206983
a_2 (a.u. /rad^4)	0.843968	0.024990	0.021187	0.380044
a_3 (a.u. /rad^2)	0.164429	0.093631	0.100454	0.074966
a_4 (a.u. /rad^4)	0.536553e-5	0.018440	0.015803	0.94550e-3
θ_{eq} (deg)	115.5630	108.9325	107.1922	115.5377

Table III(cont). Angles Fitted with Polynomials

Parameter	θ_{215} C_2-C_1-H_5	θ_{318} N-C_1-H_8	θ_{319} N-C_1-H_9
a_1 (a.u. /rad^2)	0.149579	0.063125	0.074970
a_2 (a.u. /rad^4)	0.209578	0.169919	0.086346
a_3 (a.u. /rad^2)	0.052494	0.089689	0.084323
a_4 (a.u. /rad^4)	0.103488e-2	0.214176e-6	0.148022e-6
θ_{eq} (deg)	114.7221	104.3932	107.1102

Table IV. Dihedral Angles Fitted with Cosines

	D_1 Δ_{123}- Δ_{126}	D_2 Δ_{123}- Δ_{127}	D_3 Δ_{123}- Δ_{214}	D_4 Δ_{214}- Δ_{215}	D_5 Δ_{318}- Δ_{319}
q_1 (a.u.)	-0.235211	-0.251495	0.034109	-0.064566	1.97102
q_2 (a.u.)	0.054125	0.069478	-0.124834	0.325112e-2	-1.30837
q_3 (a.u.)	-0.948188e-2	-0.020727	-0.046247	-0.250652e-2	0.57172
q_4 (a.u.)	-0.252401e-3	0.419956e-2	0.035198	0.990743e-3	-0.12758
φ_{eq} (deg)	124.22423	238.40239	12.533469	178.37286	108.39747

Table IVb. Dihedral Angle Fitted with Cosines

	D_6 Δ_{123}- Δ_{318}
q_1 (rad)	0.402832
q_2 (a.u.)	-0.109432e-01
q_3 (a.u.)	0.254772e-02
φ_{eq} (deg)	324.44275

Table V. Repulsive Energy Parameters: $E_{rep} = \frac{m_1}{r}\exp\left(-m_2 r - m_3 r^2\right)$

Parameter	Cu-H	Cu-C	Cu-N	Cu-O
m_1 (ev Å)	45.0225	116.762	426.428	642.183
m_2 (Å^{-1})	0.728702	0.885174	1.93137	2.45548
m_3 (Å^{-2})	0.691098	0.531138	0.265195	0.118378

APPENDIX A: MOLECULAR SURFACE

Each atom in the molecule is assigned a van der Waals radius enabling the molecule to be viewed as a set of interpenetrating spheres. A cylindrical axis is chosen and the molecule is "sliced" perpendicular to that axis into N imaginary planes, where N is of order 20. Each plane so formed therefore contains circles of intersection of the spheres with the plane.

A "solvent sphere" or ball of radius appropriate to the solvent (usually the radius of a water molecule) is then "rolled" over the outer circles of the plane. This solvent sphere is divided into equal segments along its circumference, typically 20-40 such pieces. Allow that we mark these segments by "x's" along the circumference. As the ball rolls around the plane, the x's touch the outer circles of the molecule, at which points we place a node or "dot". At places where the solvent sphere bridges two atoms in such a way that its x or x's lie along the bridge rather than at an atomic touching point, a dot or dots are placed at the x's themselves. In this way, the dots are uniformly distributed on the outer perimeter of the molecular plane. Each plane may contain up to M (~<200) dots.

To each of these dots we assign a unit vector, lying along the radial direction from the center of the atom associated with the dot. Care is taken to reverse the direction of the normal when the dot is derived from the solvent sphere rather than an atom of the molecule.

At this point in the calculation we have N planes containing up to M dots per plane along the perimeter. The dots are next connected between adjacent planes to form triangles which then form the surface of the molecule. One-third of the area of each triangle is then associated with each dot comprising the triangle.

The coordinates of the dots, the unit normals at each dot, and the elemental areas associated with each dot are then used in discretizing the boundary. The total surface area of the molecule is therefore computed by adding these elements and provides a reasonably accurate molecular surface area given that the van der Waals radii are known.

To find an approximate molecular volume, the radius vector from the geometrical center of each plane (this should lie along the x axis, where x is "sliced" molecular axis) to each of the dots is found. The area swept out by this radius vector as it revolves about the planar axis is then determined; that is, the area of each individual plane is found. The volume is then given simply by the (even) spacing between the planes multiplied by the total planar area.

Appendix B: Fitting the Quantum Mechanical (MP2) Energies

The individual plots of the quantum mechanical energies determined using GAUSSIAN at the MP2 level of theory for 6-31-G** wavefunctions are provided below.

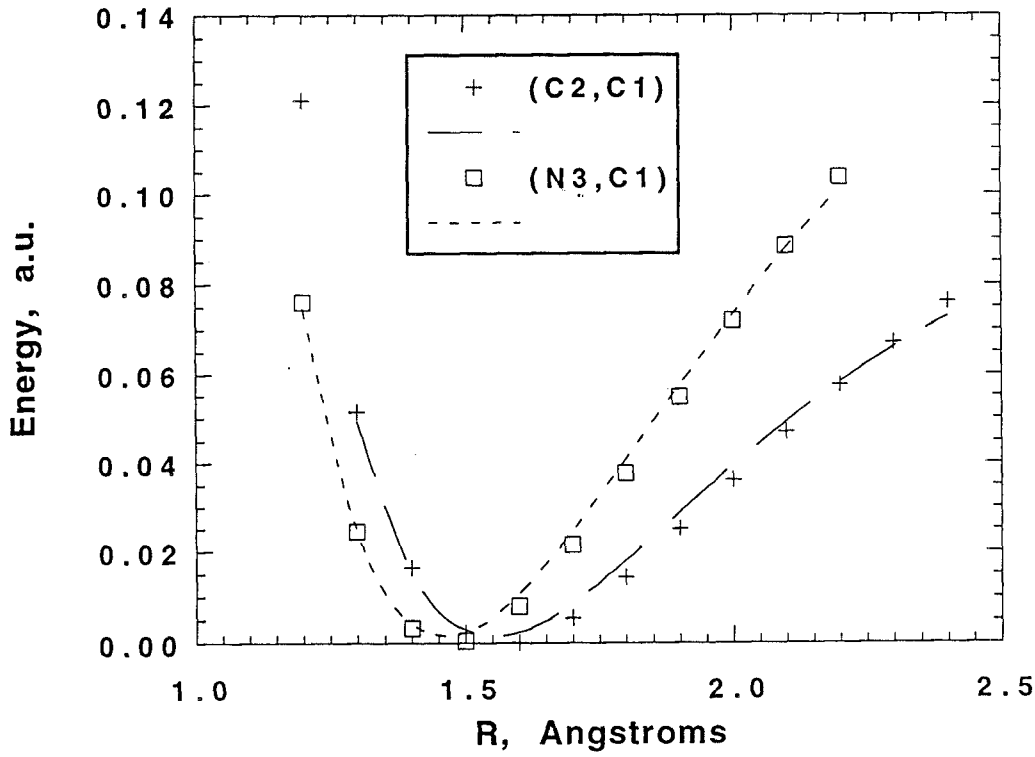

Figure B1 - Comparison of ab-initio and fitted energies vs. interatomic separations R=(C2,C1), (N3,C1) for anionic (AN) Glycine. The atom numbering is given in Figure 1a. Ab-initio calculations are indicated as points, and fitted functions shown as lines through the fitted domain.

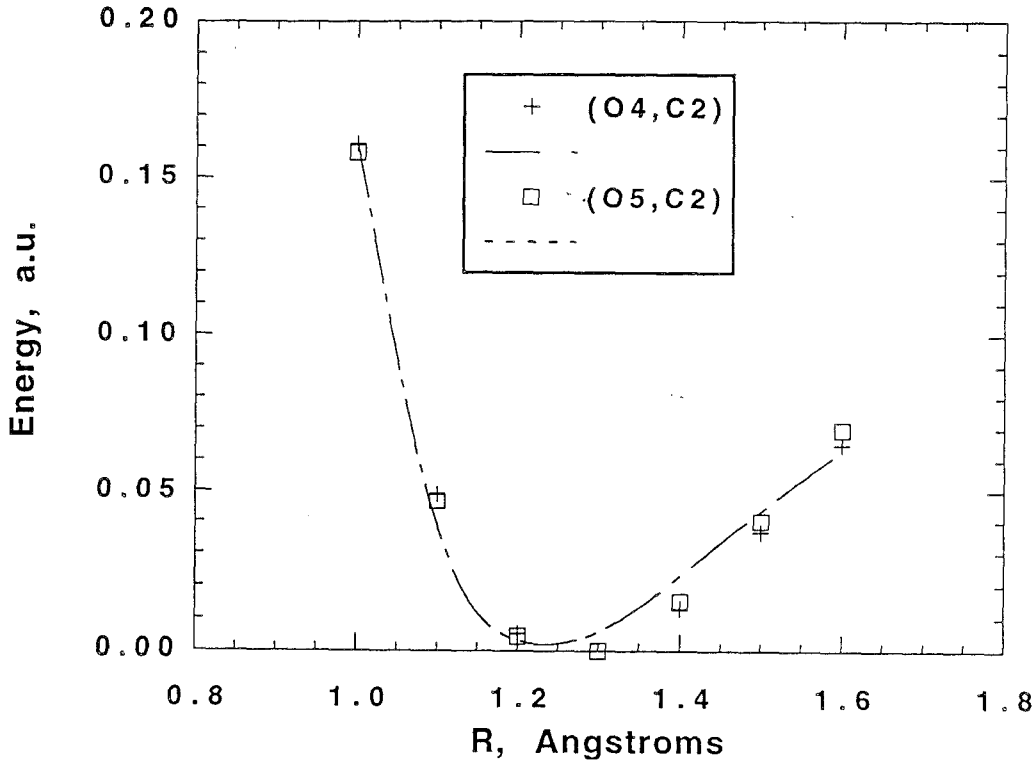

Figure B2 - Comparison of ab-initio and fitted energies vs. interatomic separations R=(O4,C2), (O5,C2) for anionic (AN) Glycine. The atom numbering is given in Figure 1a. Ab-initio calculations are indicated as points, and fitted functions shown as lines through the fitted domain.

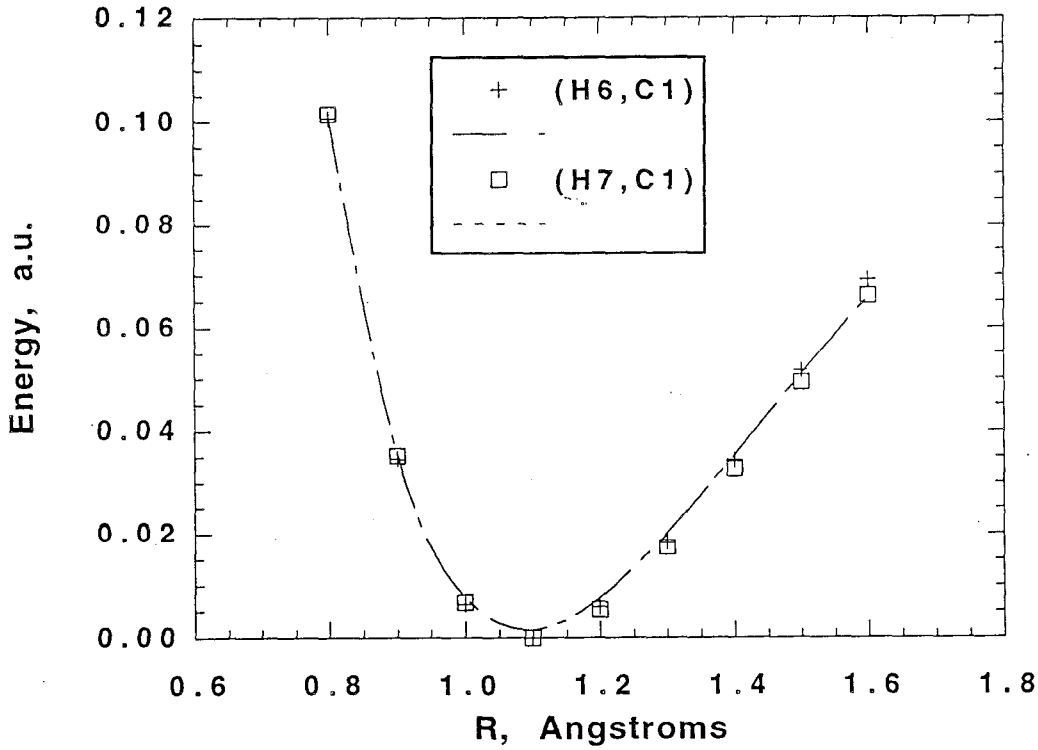

Figure B3 - Comparison of ab-initio and fitted energies vs. interatomic separations R=(H6,C1), (H7,C1) for anionic (AN) Glycine. The atom numbering is given in Figure 1a. Ab-initio calculations are indicated as points, and fitted functions shown as lines through the fitted domain.

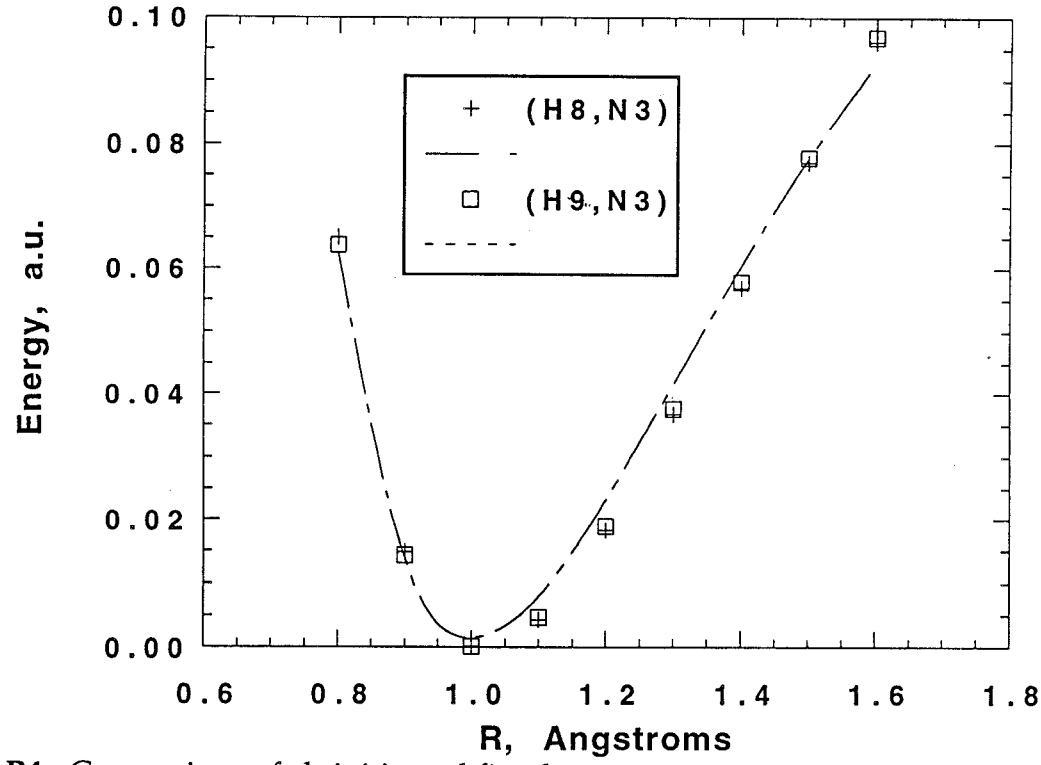

Figure B4 - Comparison of ab-initio and fitted energies vs. interatomic separations R=(H8,N3), (H9,N3) for anionic (AN) Glycine. The atom numbering is given in Figure 1a. Ab-initio calculations are indicated as points, and fitted functions shown as lines through the fitted domain.

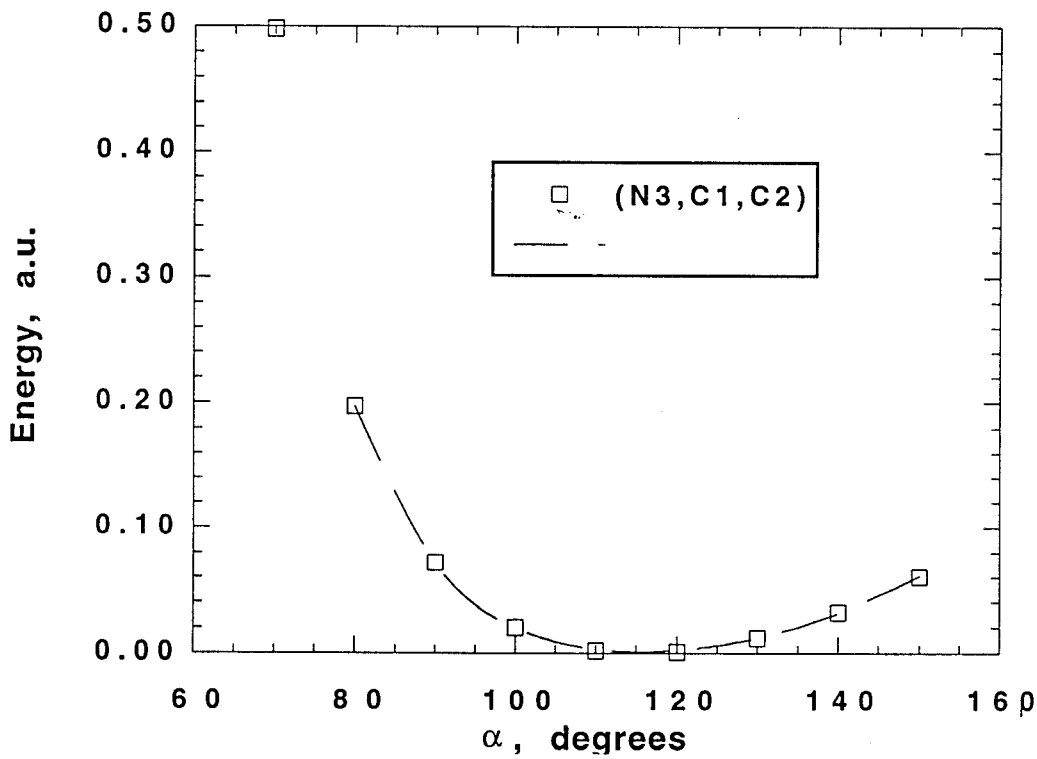

Figure B5 - Comparison of ab-initio and fitted energies vs. interatomic angle a=(N3,C1,C2) for anionic (AN) Glycine. The vertex of the included angle α at atom center C1.The atom numbering is given in Figure 1a. Ab-initio calculations are indicated as points, and fitted functions shown as lines through the fitted domain.

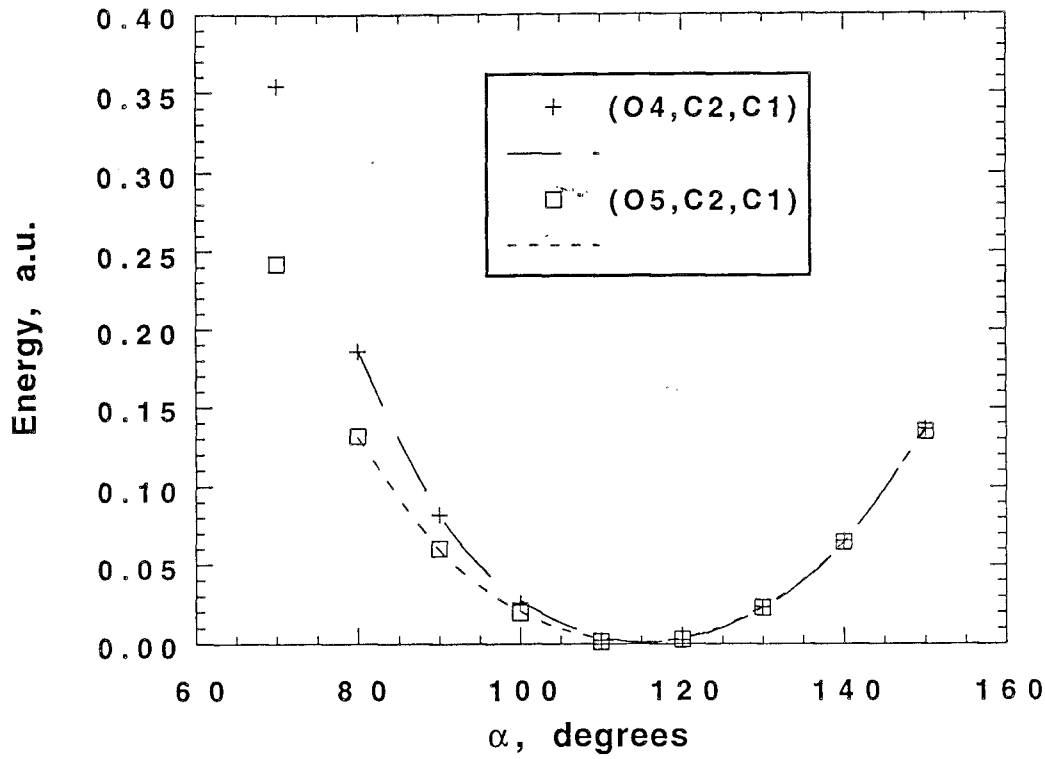

Figure B6 - Comparison of ab-initio and fitted energies vs. interatomic angles α=(O4,C2,C1), (O5,C2,C1) for anionic (AN) Glycine. The vertex of the included angles α is at atom center C2.The atom numbering is given in Figure 1a. Ab-initio calculations are indicated as points, and fitted functions shown as lines through the fitted domain.

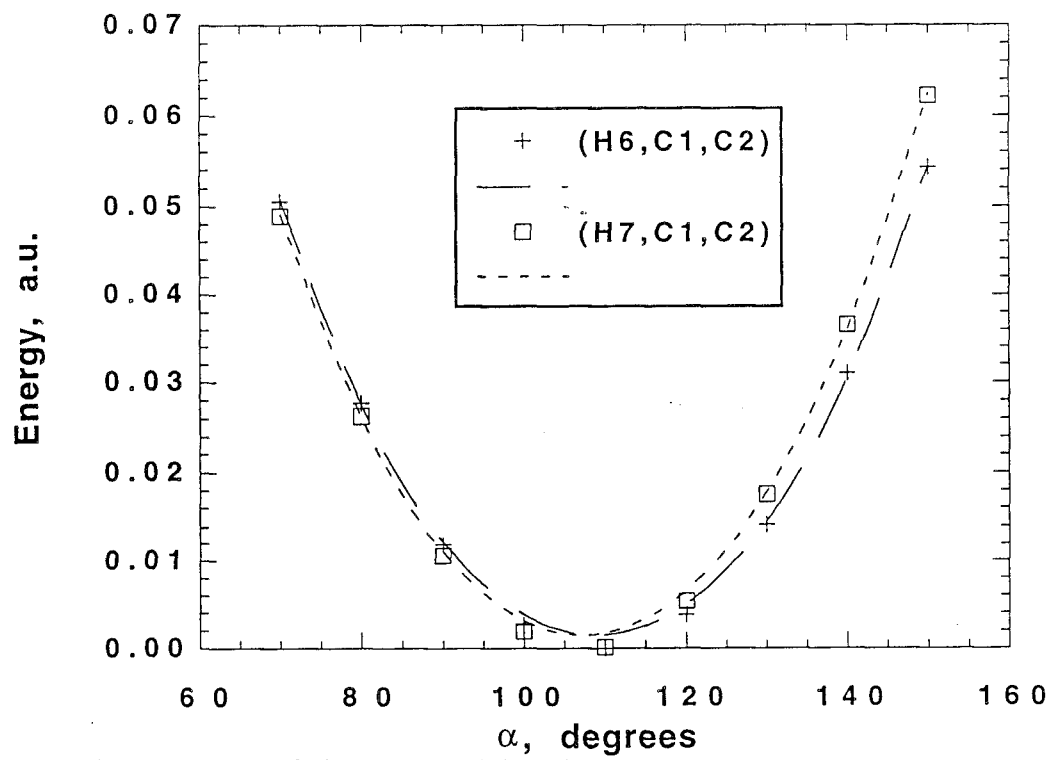

Figure B7 - Comparison of ab-initio and fitted energies vs. interatomic angles α=(H6,C1,C2), (H7,C1,C2) for anionic (AN) Glycine. The vertex of the included angles a is at atom center C1.The atom numbering is given in Figure 1a. Ab-initio calculations are indicated as points, and fitted functions shown as lines through the fitted domain.

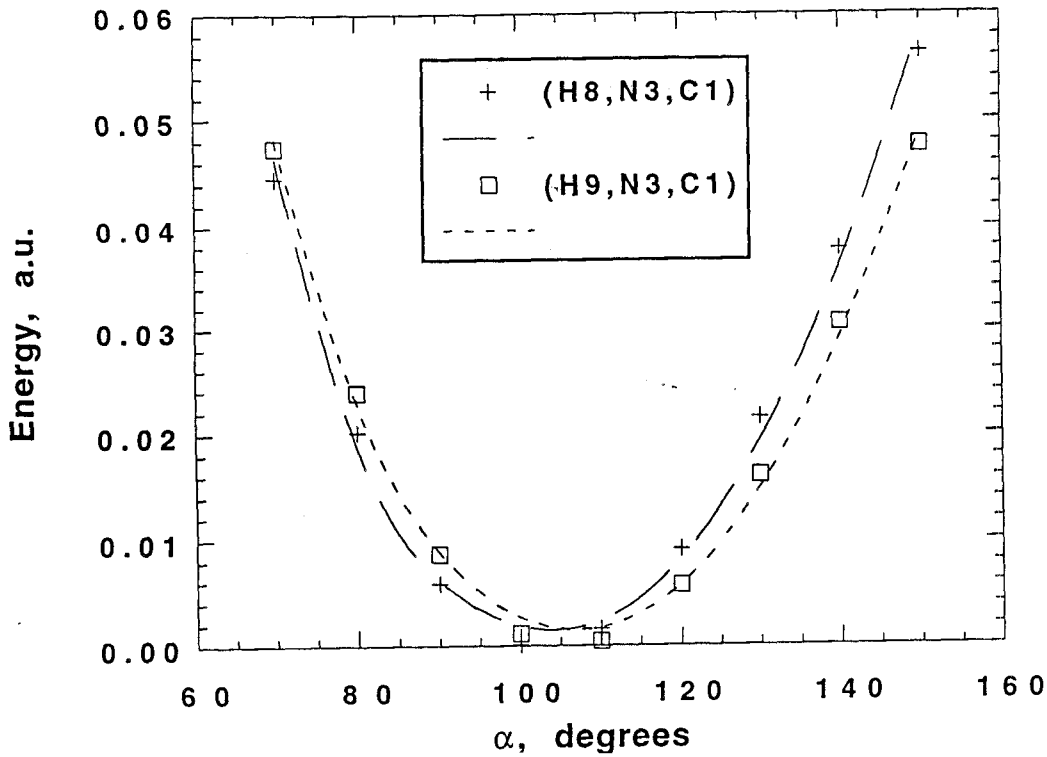

Figure B8 - Comparison of ab-initio and fitted energies vs. interatomic angles a=(H8,N3,C1), (H9,N3,C1) for anionic (AN) Glycine. The vertex of the included angles a is at atom center N3.The atom numbering is given in Figure 1a. Ab-initio calculations are indicated as points, and fitted functions shown as lines through the fitted domain.

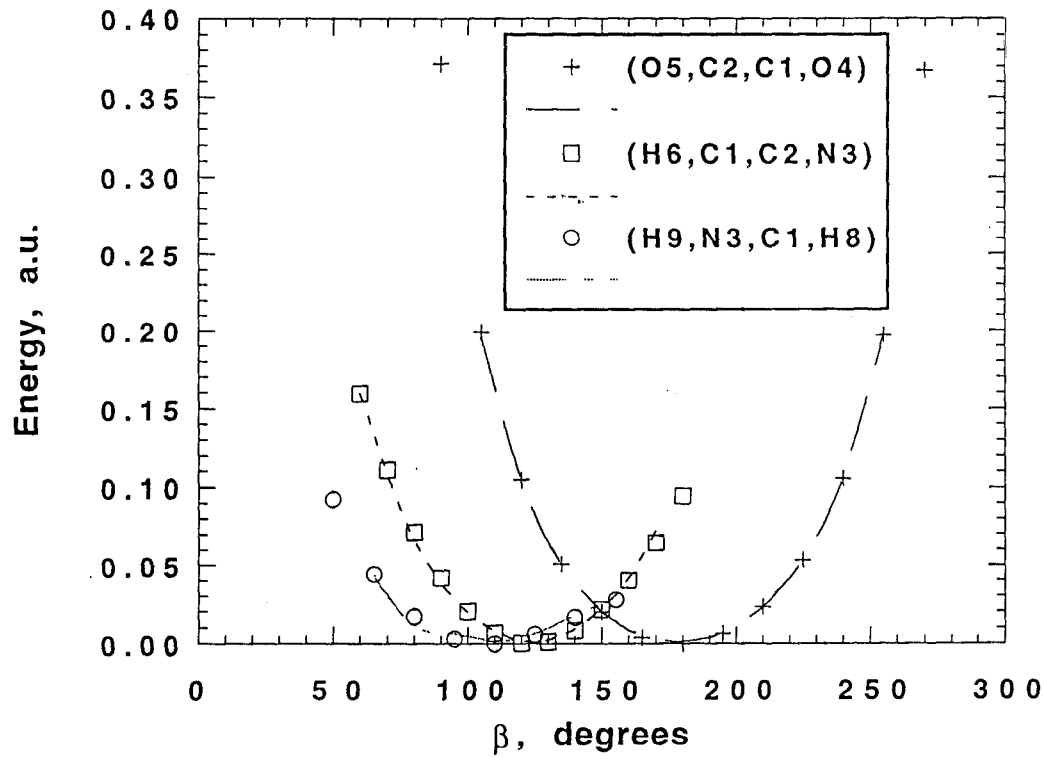

Figure B9 - Comparison of ab-initio and fitted energies vs. interatomic dihedral angles β=(O5,C2,C1,O4), (H6,C1,C2,N3) and (H9,N3,C1,H8) for anionic (AN) Glycine. The atom numbering is given in Figure 1a. Ab-initio calculations are indicated as points, and fitted functions shown as lines through the fitted domain.

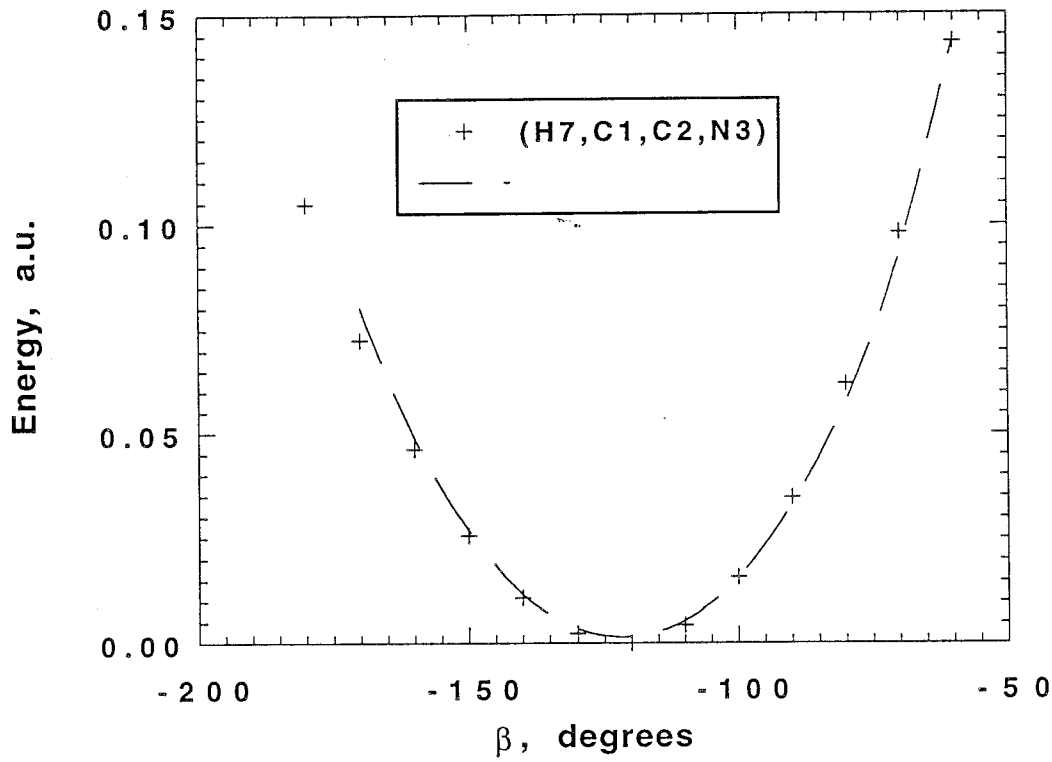

Figure B10 - Comparison of ab-initio and fitted energies vs. interatomic dihedral angle β=(H7,C1,C2,N3) for anionic (AN) Glycine. The atom numbering is given in Figure 1a. Ab-initio calculations are indicated as points, and fitted functions shown as lines through the fitted domain.

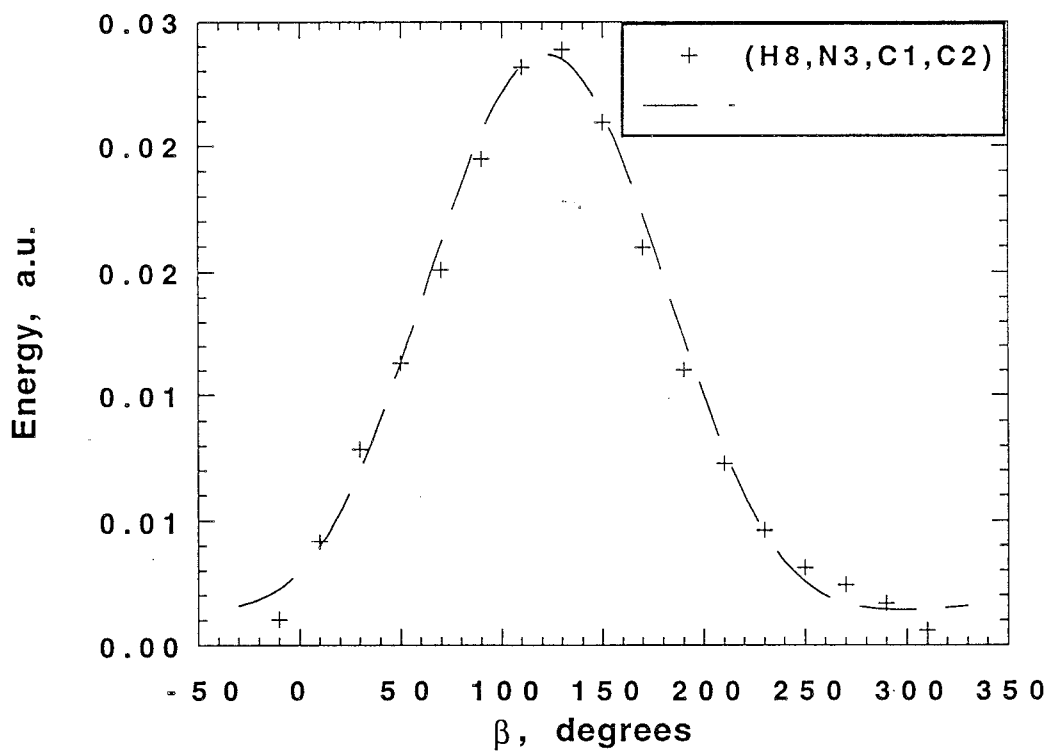

Figure B11 - Comparison of ab-initio and fitted energies vs. interatomic dihedral angle β=(H8,N3,C1,C2) for anionic (AN) Glycine. The atom numbering is given in Figure 1a. Ab-initio calculations are indicated as points, and fitted functions shown as lines through the fitted domain.

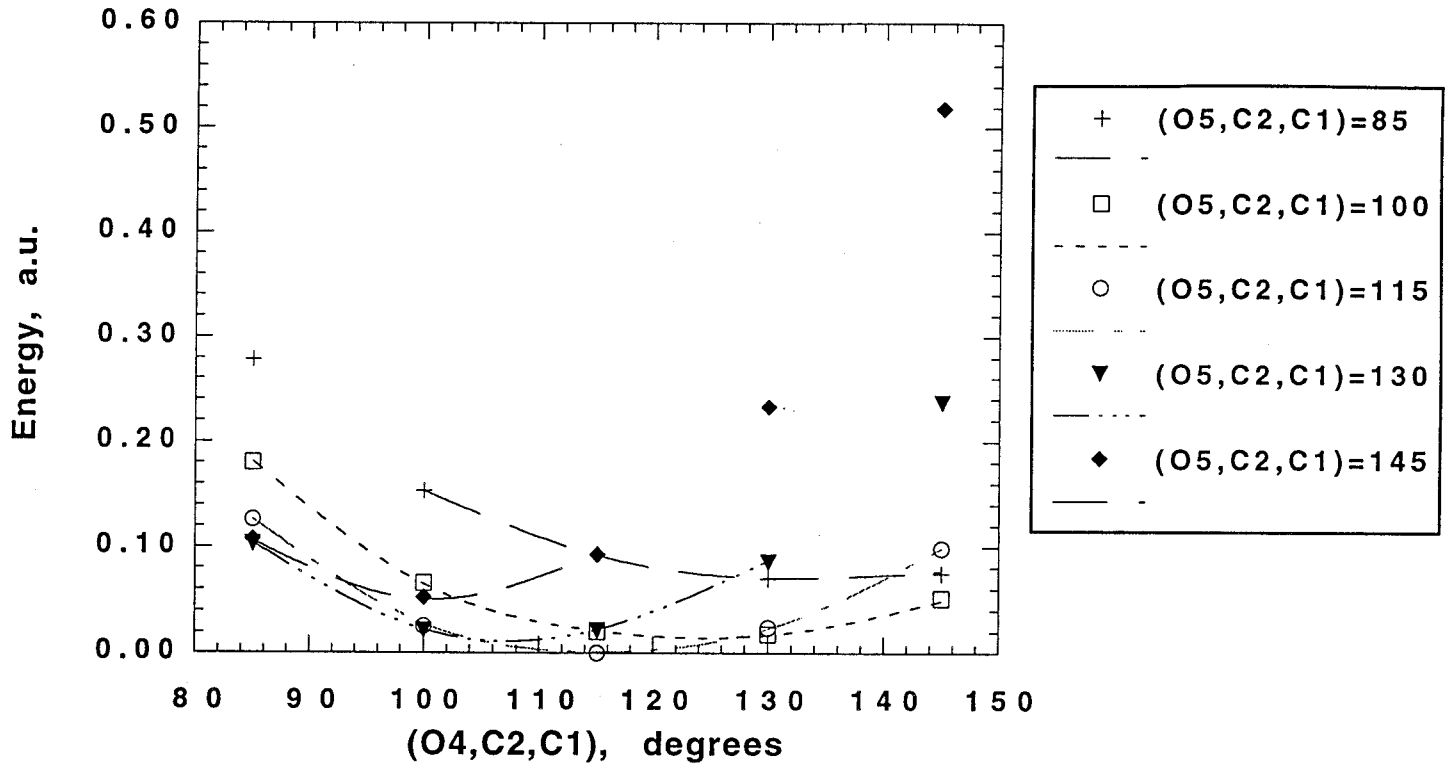

Figure B12 - Comparison of ab-initio and fitted energies vs. interatomic angles α=(O4,C2,C1), (O5,C2,C1) for anionic (AN) Glycine. The vertex of the included angles α is at atom center C2. The atom numbering is given in Figure 1a. Ab-initio calculations are indicated as points, and fitted functions shown as lines through the fitted domain.

REFERENCES

1. J. Lausmaa, *Cellular Responses to Implanted Materials*, in Proceedings of Conference on Biomaterials:, University of California, San Diego, Institute of Mechanics and Materials Report No.94-29, 1994.

2. K. Uvdal, P. Bodo, A. Ihs, B. Liedberg and W R. Salanek, *J. Colloid and Interface Science* **140**, 207 (1990).

3. A. Ihs, B. Liedberg, K. Udval, C. Tornkvist, P. Bodo, and I. Lundstrom, *J. Colloid and Interface Science* **140**, 192 (1990).

4. B. Liedberg, I. Lundstrom, C. R. Wu, and W. R. Salaneck, *J. Colloid and Interface Science* **108**, 123 (1985).

5. C. R. Wu, J. O. Nilsson, and W. R Salaneck, *Physica Scripta*, **35**, 586 (1987).

6. L. Vroman and A L. Adams, *J. Biomed. Mater. Res.*, **3**, 43 (1969)

7. R. S. Greco, ed. *Implantation Biology*, (CRC Press, Boca Raton, 1994).

8. I. Lundstrom and W. R. Salaneck, *J. Colloid and Interface Science* **108**, 288 (1985).

9. V. Barone, C. Adamo, A. Grand, and R. Subra, *Chem. Phys. Letters*, **242**, 351 (1995).

10. Y. Ding and K. Krogh-Jesperson, *Chem. Phys. Letters*, **199**, 261 (1992).

11. GAUSSIAN 92; M. J. Frisch, et al , Gaussian, Inc., Pittsburgh PA

12. GAMMESS: J. Comput. Chem. 14, 1347 (1993).

13. SPARTAN version 4.0, Wavefunction, Inc., Irvine, CA, 92715.

14. R. J. Zauhar and R. S. Morgan, *J. Mol. Biol.* **186**, 815 (1985). (See also *J. Comp. Chem.* **11**, 603 (1990); *J. Comp. Chem.* **9**, 171 (1988); *J. Comp. Chem.* **12**, 575 (1991).

15. J. D. Jackson, *Classical Electrodynamicss*, (John Wiley and Sons, New York, 1962).

16. W. D. Wilson and C. L. Bisson, *Phys. Rev.* **B3**, 3984 (1971). (A similar method was independently introduced by R. G. Gordon and Y. S. Kim, *J. Chem. Phys.* **56**, 3122 (1972).)

17. F. Herman and S. Skillman, *Atomic Structure Calculations*, (Prentice-Hall, Inc., Englewood Cliffs, New Jersey, 1963).

18. M. L. Connolly, *J. App. Cryst*, **16**, 548 (1983).

19. M. W. Finnis, *Acta Metall. Mater. Suppl.* **40**, S25 (1992).

20. D. M. Duffy, J. H. Harding and A. M. Stoneham, *Phil. Mag. A*, **67**, 865 (1993).

21. M. E. Colvin and C. F. Melius, SAND 93-8239 (1993).

22. K. Christmann and G. Ertl, *Surface Science*, **60**, 365 (1976).

ACKNOWLEDGMENTS

The authors are grateful to Dr. Carl Melius for numerous helpful and motivating discussions. The authors also wish to thank Prof. Jukka Lausmaa of Chalmers University, Gothenburg for communicating many very exciting experimental results .

UNLIMITED RELEASE
INITIAL DISTRIBUTION

Prof. Jukka Lausmaa
Chalmers University
Gothenburg

C. M. Schaldach (5)
University of California
Berkeley, California

MS1436 L. Lopez, 4523
MS9001 T. O. Hunter, 8000
Attn: J. B. Wright, 2200, MS9005
E. E. Ives, 5200, MS9006
L. A. West, 8200, MS9420
W. J. McLean, 8300, MS9054
R. C. Wayne, 8400, MS9007
P. N. Smith, 8500, MS9002
L. A. Hiles, 8800, MS9141
D. L. Crawford, 8900, MS9003

MS9004 M. E. John, 8100
Attn: W. R. Bolton, 8102, MS9104
M. Lapp, 8102, MS9104
J. Vitko, 8102, MS9104
S. C. Johnston, 8103, MS9141
R. L. Rinne, 8104, MS9141
G. A. Thomas, 8111, MS9103
L. D. Brandt, 8112, MS9201
P. K. Falcone, 8114, MS9201
G. C. Story, 8115, MS9104
R. L. Bierbaum, 8116, MS9202

MS9214 C. F. Melius, 8117
MS9214 L. M. Napolitano, 8117
MS9214 C. L. Bisson, 8117 (5)

MS9401 T. M. Dyer, 8700
Attn: M. W. Perra, 8711, MS9402
J. C. F. Wang, 8713, MS9403
G. J. Thomas, 8715, MS9402
K. L. Wilson, 8716, MS9162
W. G. Wolfer, 8717, MS9163
G. A. Benedetti, 8741, MS9042
P. E. Nielan, 8742, MS9042
M. L. Callabresi, 8743, MS9401
W. A. Kawahara, 8746, MS9042

MS9904 W. D. Wilson, 8700 (5)
MS9403 M. I. Baskes, 8712

MS9021 Technical Communications Department, 8815/Technical Library, MS0899, 13414
MS0899 Technical Library, 13414 (4)
MS9018 Central Technical Files, 8950-2 (3)